Available online at www.sciencedirect.com
SCIENCE DIRECT®
Geochimica et Cosmochimica Acta 70 (2006) 723–741
Geochimica
www.elsevier.com/locate/gca

Multi-stage mixing in subduction zones: Application to Merapi volcano (Java island, Sunda arc)

Vinciane Debaille [a], Régis Doucelance [a,*], Dominique Weis [b,1], Pierre Schiano [a]

[a] *Laboratoire Magmas et Volcans, OPGC-Université Blaise Pascal-CNRS, 5 rue Kessler, 63038 Clermont-Ferrand Cedex, France*
[b] *Département des Sciences de la Terre et de l'Environnement, Université Libre de Bruxelles, CP 160/02, 1050 Brussels, Belgium*

Received 28 April 2005; accepted in revised form 29 September 2005

Abstract

Many studies have argued for the contribution of at least three components, namely the mantle wedge, the subducted oceanic crust, and its sediment cover, to describe the geochemistry of island arc volcanics. However, isotope correlations reflecting a simple binary mixing can be observed at the scale of a single arc island or volcano. Here we investigate the possibility that these trends reflect pseudo-binary mixing relationships in a three-component system. We present a simplified, two-stage model for the systematic isotope modelling of a cogenetic suite of arc lavas. This includes metasomatism of portions of the mantle wedge by hydrous phases released from the downgoing oceanic crust, and sediments, followed by progressive mixing and melting. A consequence of this model is that it leads to a two end-member mixing process from the mantle wedge, oceanic crust, and sediment components. To solve the model we reduce it to a step-by-step procedure combined with a Monte-Carlo simulation. The procedure consists of: (i) producing a large number of random values on each variable of the model; (ii) using the computed values to calculate the isotopic compositions of lavas; and (iii) comparing the obtained isotopic compositions with measured data. Applied to a new set of Sr, Nd, and Pb isotope data for volcanics (basalts, basaltic andesites, trachybasalts, and basaltic trachyandesites) from Merapi volcano (Java island, Sunda arc), the model successfully reproduces the binary mixing relationships previously documented for the medium-K and high-K lava series from this volcano, thus giving further support to the hypothesis that this distinction is inherited from the primary magmas and primarily reflects a property of the mantle source. The results allow identification of a set of numerical values for bulk partition coefficients (solid/hydrous fluid, and solid/H_2O-rich melt) and variables (e.g., the mass ratio between the metasomatizing phase and the mantle wedge), which can be used for quantitative arc-lava petrogenetic calculations. They also require a direct relationship between dehydration of the slab and melting of the metasomatized mantle wedge. Finally, our evaluation shows that for isotope modelling of the Merapi lavas, the two-stage procedure is controlled more by the considered source components (mantle wedge, oceanic crust, sediments, and their derivatives) than by the various processes involved (dehydration, melting, and mixing).

1. Introduction

Geochemical characteristics of island-arc basalts (IAB) are consistent with derivation by partial melting of portions of the upper mantle that have been enriched in water and incompatible elements due to interaction with a H_2O-rich phase released from subducted oceanic lithosphere (e.g., Gill, 1981). The trace-element characteristics of IAB (depletion of high field strength elements, HFSE, relative to the large ion lithophile elements, LILE) reflect this enrichment process (e.g., Perfit et al., 1980; Saunders et al., 1980; Arculus and Powell, 1986; McCulloch and Gamble, 1991). The enrichment process operates on mantle sources which are believed to be depleted peridotites, comparable to the source of mid-ocean ridge basalts (MORB). However, some arc magmas have been proposed to form by melting non-peridotite sources, such as ocean island basalt (OIB)-type source (Morris and Hart, 1983; Ito and

* Corresponding author. Fax: +33 4 73 34 67 44.
E-mail address: doucelance@opgc.univ-bpclermont.fr (R. Doucelance).
[1] Pacific Centre for Isotopic and Geochemical Research, Department of Earth and Ocean Sciences, University of British Columbia, Vancouver, Canada V6T 1Z4.

0016-7037/$ - see front matter © 2005 Elsevier Inc. All rights reserved.
doi:10.1016/j.gca.2005.09.021

Stern, 1986), subducted crust (Kay, 1978; Defant and Drummond, 1990), deep crust (Pichler and Zeil, 1972), and lower crustal or shallow upper mantle clinopyroxene-rich cumulates (Schiano et al., 2000). In addition, although coupled metasomatism and fluxed melting of peridotites in the mantle wedge is believed to be the dominant process by which primary arc magmas form and acquire their distinctive geochemical signature (e.g., McCulloch and Gamble, 1991; Stolper and Newman, 1994), important aspects of this process remain somewhat hypothetical.

In particular it is still not clear whether the high concentrations of LILE elements in arc lavas directly reflect their relative solubilities in slab-derived hydrous fluids (Tatsumi et al., 1986; Keppler, 1996), or are controlled by the subducted sediment input (Plank and Langmuir, 1993). In fact some of the geochemical characteristics of IAB, particularly their high Pb isotope ratios (Kay, 1978; White, 1985), high Sr isotope ratios (Perfit et al., 1980; McLennan and Taylor, 1981; White and Patchett, 1984; Hawkesworth et al., 1993) and the presence of ^{10}Be (Tera et al., 1986), are attributed to recycled sediment contributions to the lava source. However, it has been shown that the geochemical characteristics of some arc lavas, for example from the Kamchatka arc (Kersting and Arculus, 1995), do not require the presence of recycled sediments in their source. In any case, it is still a matter of debate how reliably recycled sediment contributions to the source can be distinguished from crustal contamination during shallow level fractional crystallization. Finally, subduction zones act as a dynamic system, in which motion rate of the slab may vary in time, and variation in the sediment accumulation rate on the oceanic floor may modify the potential sediment supply to the subduction zone (Alves et al., 1999). The extent to which the observed compositional variations among arc volcanics reflect the above influences remains poorly understood.

Many authors have argued for the contribution of three components, namely the mantle wedge, the subducted basaltic ocean crust and its sediment cover, to account for the geochemistry of arc basalts (e.g. Kay, 1980; Ellam and Hawkesworth, 1988; Miller et al., 1994; Turner et al., 1996). However, even if arc lavas do not define an overall trend on isotope variation diagrams such as the "mantle-array" for MORB and OIB, correlations reflecting a simple binary mixing can be observed at the scale of a single arc island or volcano (e.g., Ellam and Hawkesworth, 1988; Turner et al., 1997; Turner and Foden, 2001). This observation seems, at first sight, to challenge the variety of physical processes and element fluxes that could be involved in the generation of arc magmas, as well as the number of potential sources. It suggests the predominance of two sources linked by a simple process of mixing. An alternative explanation is that the correlations for arc lavas are pseudo-binary mixing lines, formed by mixing of three or more components, as documented for basalts from some mid-ocean ridge regions (Hanan et al., 1986; Schilling et al., 1992; Douglass and Schilling, 2000).

In this paper, we present a two-stage model for the systematic isotope modelling of a cogenetic suite of arc lavas. The first stage of the model considers metasomatism of portions of the mantle wedge by hydrous fluids and/or melts derived from dehydration and/or melting reactions in the down-going altered oceanic crust and sediments. These processes lead to the definition of two end-members, namely the portions of mantle wedge metasomatized by the oceanic crust-derived phase and those metasomatized by the sediment-derived phase. The second stage of the model concerns progressive mixing of the two end-members thus defined. An important consequence of this two-stage model is that it leads to a two end-member mixing process from three distinct components (the mantle wedge, the subducted, altered oceanic crust, and sediments). For the purpose of testing, we apply the model to a new set of isotopic data (Sr, Nd, and Pb) for volcanics from Merapi volcano (Java island, Sunda arc), combining step-by-step calculations with a Monte-Carlo approach. Merapi volcano is almost ideally suited to be a case study for several reasons. Geochemical characteristics of the lavas might be ascribed to variable amounts of recycled oceanic crust and sediments in the source (McDermott and Hawkesworth, 1991; Alves et al., 1999; Turner and Foden, 2001; Gertisser and Keller, 2003a), contamination by the overlying basement does not significantly affect their whole-rock isotopic compositions and compositional correlations reflecting binary mixing relationships are documented (Alves et al., 1999; Gertisser and Keller, 2003a). The results show that the multi-stage model proposed here can reproduce the binary mixing trends defined by Merapi lavas. They also give a set of numerical values for bulk partition coefficients (solid/hydrous fluid, and solid/H_2O-rich melt) and parameters such as the mass ratio between the metasomatizing phase and the mantle wedge, which can be used for quantitative arc-lava petrogenetic calculations.

2. Role of subducted oceanic crust and sediments in arc lava petrogenesis

Evaluation of the influence of dehydration/melting of slab components on the generation of arc lavas is limited by imperfect knowledge of parameters such as the thermal structure of the upper mantle beneath volcanic arcs (e.g., Tatsumi et al., 1983) and the mineralogy of the subducted materials. Two parts of the descending slab can potentially play an important role in arc magma genesis: the altered oceanic crust and its sediment cover (Fig. 1).

Correctly assessing the contribution of the subducted oceanic crust, either as hydrated fluids or as silicate melts, to source regions of arc volcanics has been the subject of several studies (e.g., Kay, 1980; Perfit et al., 1980; Wyllie, 1982; Von Drach et al., 1986; Tatsumi et al., 1986; Woodhead, 1989; Davies and Stevenson, 1992; Schiano et al., 1995; Elliot et al., 1997; Yogodzinski and Kelemen,

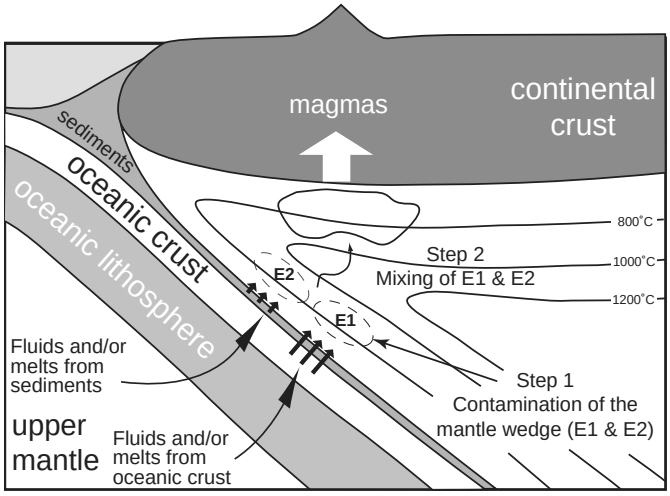

Fig. 1. Schematic cross section of the mantle wedge beneath a subduction zone illustrating the model of formation of arc lavas discussed in the text. Stage 1 considers metasomatism of the mantle wedge by fluids and/or melts derived by dehydration and/or melting processes in the down-going altered oceanic crust and sediments. Stage 2 considers progressive mixing of the two distinct end-members E1 and E2: E1, the portions of mantle wedge metasomatized by the phase issued from the subducted oceanic crust, and E2, the portions of mantle wedge metasomatized by the phase issued from the subducted sediments.

1998). Direct partial melting of the oceanic crust, thought to generate geochemically distinct andesitic lavas (Kay, 1978; Defant and Drummond, 1990), is generally restricted to young subduction/collision zones, incipient subduction, or post-collisional regimes, during thermal re-equilibration following cessation of subduction (e.g., Peacock, 1990; Davies and Stevenson, 1992; Peacock et al., 1994; Iwamori, 1998). Direct evidence for slab melting is given by the study of olivine-hosted melt inclusions in xenoliths from sub-arc mantle regions, which sample H_2O-rich silicate melt phases whose chemistry indicates an origin by very low degrees of melting of the subducted oceanic crust (Schiano et al., 1995). The aqueous fluid and/or silicate melt phase released from the subducted oceanic crust is generally considered to induce coupled metasomatism and fluxed melting of peridotites in the mantle wedge (e.g., Nicholls and Ringwood, 1973; Tatsumi et al., 1986). An alternative is that the phase does not directly trigger melting of the mantle wedge, as it reacts with the overlying peridotites that are then dragged downward above the subducting slab by the viscous coupling between the mantle wedge and the rigid slab (Tatsumi and Kogiso, 1997).

Subducted sediments, if present, can also be dehydrated and/or melted. Experiments indicate that melting of pelagic sediments occurs at a slightly lower temperature than wet gabbro (Nichols et al., 1994), thus sediment melting and subducted gabbroic crust dehydration can occur at the same temperature. This observation can be linked to the deduction of Plank and Langmuir (1993) that in many subduction zones the proportion of silicate melts released by subducted sediments is much more important than altered oceanic crust.

2.1. Behaviour of trace elements during dehydration and melting

When the descending plate, capped with hydrated oceanic crust and sediments, is warmed up by the surrounding mantle, high T/high P metamorphism takes place. Dehydration governed by the breakdown of hydrous phases, and possibly by the melting of descending material occurs at particular depths (Fig. 1). The resulting fluids and melts released from the slab act as an important means of mass transfer from the slab to the mantle wedge and are often invoked in order to explain many of the geochemical characteristics of arc magmas. However, assessing the exact influence of such mass transfer on island-arc characteristics requires precise evaluation of the chemical behaviour of elements in the released phase. As discussed below, behaviour of trace elements during dehydration and melting processes is directly related to their mobility and solid/melt partition coefficients, respectively.

2.1.1. Relationship between slab-derived fluids and melts

Evidence for the identity and composition of the phase(s) released from subducted oceanic lithosphere is mostly indirect, based primarily on the chemical compositions of erupted arc lavas and mineral/fluid partitioning experiments that provide insight into the compositional characteristics of slab-derived fluids. Therefore there are still some aspects of the processes that transport the elements from the slab to the sources of arc lavas which remain somewhat hypothetical. For example, unambiguous characterization of the primary phase (fluid and/or melt) has proven to be difficult. Some authors have proposed complete miscibility between hydrous fluids and silicate melts at upper mantle P–T conditions (Bureau and Keppler, 1999), whereas others have suggested partial miscibility, broadly controlled by the amount of Cl in the fluid (Ayers and Eggler, 1995). The amount of dissolved silica in aqueous fluids at these temperatures and pressures does not have a major effect on mineral-aqueous fluid partitioning of trace elements (Keppler, 1996), because it is mainly controlled by the crystal chemistry of the residual phase (Stalder et al., 1998). Thus, only small differences in trace-element partitioning between aqueous fluids and silicate melts are expected, except perhaps for Th, Be, and Nb (Jonhson and Plank, 1999), and the geochemical signature left by the fluids will not be distinctly different from that of silicate melts (Ayers and Eggler, 1995). However, in the following investigations we will still separate the slab-derived metasomatic phase into (i) hydrous fluids and (ii) silicate melts.

2.1.2. Dehydration

Transport of a trace element (x) during dehydration is related to its ability to be dissolved into aqueous fluids. The mobility (M^x) of x can thus be expressed as the amount of x lost during dehydration divided by its initial value (Tatsumi et al., 1986)

$$M^x = \frac{C_o^x - C_{\text{run}}^x}{C_o^x}, \tag{2.1}$$

where C_{run}^x is the concentration of element x after dehydration, and C_o^x, its initial concentration in the slab components (oceanic crust and sediments).

Assuming an equilibrium-state dehydration process, the mass balance equation gives

$$C_o^x = f \times C_{\text{fluids}}^x + (1-f) \times C_{\text{run}}^x, \tag{2.2}$$

where f is the weight fraction of hydrous fluids extracted from the slab components and C_{fluids}^x the concentration of element x into these fluids.

By rearranging Eqs. (2.1 and 2.2) we obtain

$$C_{\text{fluids}}^x = \frac{C_o^x}{f} \times [1 - (1-f) \times (1 - M^x)]. \tag{2.3}$$

A fundamental assumption underlying the use of radiogenic (e.g., Sr, Nd, and Pb) isotopes is that dehydration processes do not fractionate them. Thus, the isotopic composition of long-lived isotopes of heavy elements in slab-derived fluids (α_{fluids}^x) and subducted materials (α_o^x) should be the same

$$\alpha_{\text{fluids}}^x = \alpha_o^x. \tag{2.4}$$

2.1.3. Melting

The behaviour of trace element x during melting is expressed by the bulk solid/melt partition coefficient (D^x)

$$D^x = \frac{C_{\text{solid}}^x}{C_{\text{melt}}^x}, \tag{2.5}$$

where C_{solid}^x and C_{melt}^x are the concentrations of element x in the slab components and silicate melts, respectively.

Assuming equilibrium-state melting, the mass balance equation gives the initial concentration (C_o^x) of element x in the subducted materials

$$C_o^x = F \times C_{\text{melt}}^x + (1-F) \times C_{\text{solid}}^x, \tag{2.6}$$

where F is the melt fraction.

Thus, combining Eqs. (2.5 and 2.6), the equation for the concentration of trace element x in a silicate melt is

$$C_{\text{melt}}^x = \frac{C_o^x}{D^x + F \times (1 - D^x)}. \tag{2.7}$$

As in the case of dehydration, long-lived isotopes of heavy elements are not fractionated during melting; isotopic compositions of slab-derived melts ($\alpha_{\text{melt}}{}^x$) are thus in equilibrium with their source

$$\alpha_{\text{melt}}^x = \alpha_o^x, \tag{2.8}$$

where α_o^x is the isotopic composition of the subducted materials.

3. Modelling procedure

Important features of IAB isotope compositions, which should be explained by any global subduction zone model, are the binary mixing relationships that can be observed at the scale of a single island or volcano (e.g., Ellam and Hawkesworth, 1988; Turner et al., 1997; Turner and Foden, 2001; Alves et al., 2002). To address this characteristic, we use the following two-stage model to approximate the formation of arc magmas (Fig. 2).

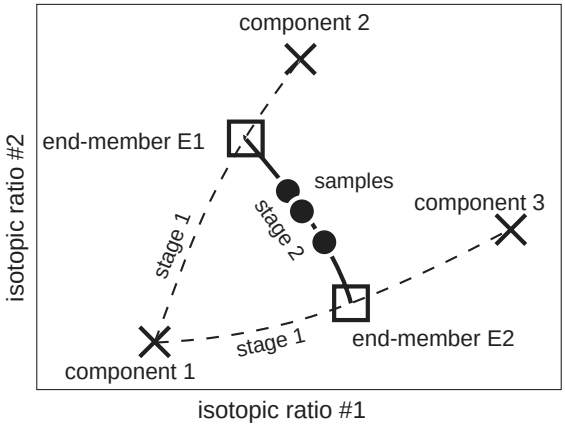

Fig. 2. Isotope diagram showing a hypothetical curved data array resulting from mixing of the two end-members E1 and E2 in a three component system, referred to as a pseudo-binary mixing array.

In the first stage, metasomatism of the mantle wedge by hydrous fluids and/or silicate melts derived from dehydration and/or melting reactions in the down-going slab generates two distinct end-members: E1, the portion of mantle wedge metasomatized by melts/fluids issued from the subducted oceanic crust, and E2, the portion of mantle wedge metasomatized by melts/fluids issued from the subducted sediments. An important observation to be made is that this first stage reduces the three involved components (mantle wedge, oceanic crust, and sediments) to two end-members.

In the second stage, after some unspecified period of time, the two end-members (E1 and E2) are mixed and melted to generate arc lavas.

It should be noted that contamination via assimilation of continental crust through the assimilation-fractional crystallization model (AFC, DePaolo, 1981) could also affect the isotopic composition of arc magmas. How reliably such shallow-level crustal contamination may be distinguished from recycled sediment contributions to the magma source is still a matter of debate (e.g., Davidson, 1987; Davidson et al., 2005).

A recent study of Merapi samples by Chadwick et al. (2005) has provided evidence for crustal influence at the mineral scale. However, in the case of Java, a significant role of the crustal contamination on the whole-rock isotopic compositions was previously dismissed (Alves et al., 1999, 2002; Gertisser and Keller, 2003a). For this reason, and also because there are subduction zones which do not have a continental basement, we decided not to consider crustal contamination in our modelling.

3.1. Mathematical formulation

3.1.1. Dehydration and melting of subducted materials

Using Eqs. (2.3 and 2.7), we obtain the concentration ($C^x_{OC/SED}$) of element x in the melts/fluids originating from melting/dehydration of subducted oceanic crust (C^x_{OC}) and sediments (C^x_{SED})

$$C^x_{OC/SED} = \frac{Tm}{Tm+1} \times C^x_{melt} + \frac{1}{Tm+1} \times C^x_{fluid}, \quad (3.1)$$

where Tm is the mass ratio between melts and hydrous fluids issued from melting and dehydration reactions in the slab.

From the definition of the mass ratio Rm between the slab-derived melts/fluids and the mantle wedge, we can determine the concentration of element x ($C^x_{end\text{-}member}$) in the end-members E1 and E2 (the mantle wedge contaminated by melts/fluids issued from subducted oceanic crust and sediments, respectively)

$$C^x_{end\text{-}member} = \frac{Rm}{Rm+1} \times C^x_{OC/SED} + \frac{1}{Rm+1} \times C^x_{MW}, \quad (3.2)$$

where C^x_{MW} is the concentration of element x in the mantle wedge.

For the isotopic compositions of E1 and E2, we consider Eqs. (2.4 and 2.8) and use a complete formulation of mixing, to take into account potentially large differences in isotopic compositions between slab-derived melts/fluids and the mantle wedge

$$\alpha^x_{end\text{-}member} = \gamma_\alpha \times \alpha^x_o + (1-\gamma_\alpha) \times \alpha^x_{MW}, \quad (3.3)$$

where α^x_{MW} is the isotopic composition of the mantle wedge and γ_α the mass fraction of the normalizing isotope for the isotopic ratios $\alpha^x_{end\text{-}member}$, α^x_o, and α^x_{MW}

$$\gamma_\alpha = \frac{\dfrac{Rm \times C^x_{OC/SED}}{1+\left(\sum_{i=1}^{n} \frac{a_i}{b} \times \frac{Ma_i}{Mb}\right)_{OC/SED}}}{\dfrac{Rm \times C^x_{OC/SED}}{1+\left(\sum_{i=1}^{n} \frac{a_i}{b} \times \frac{Ma_i}{Mb}\right)_{OC/SED}} + \dfrac{C^x_{MW}}{1+\left(\sum_{i=1}^{n} \frac{a_i}{b} \times \frac{Ma_i}{Mb}\right)_{MW}}}, \quad (3.4)$$

where $\left(\sum_{i=1}^{n} a_i/b \times M_{a_i}/M_b\right)_{OC/SED}$ and $\left(\sum_{i=1}^{n} a_i/b \times M_{a_i}/M_b\right)_{MW}$ correspond to the isotopic compositions of slab-derived melts/fluids and the mantle wedge, respectively, weighted by the ratios of molar masses. For instance, this gives for Pb

$$\frac{^{206}Pb}{^{204}Pb} \times \frac{M_{^{206}Pb}}{M_{^{204}Pb}} + \frac{^{207}Pb}{^{204}Pb} \times \frac{M_{^{207}Pb}}{M_{^{204}Pb}} + \frac{^{208}Pb}{^{204}Pb} \times \frac{M_{^{208}Pb}}{M_{^{204}Pb}}. \quad (3.5)$$

3.1.2. Mixing of end-members

Given the concentrations and isotopic compositions of end-members E1 and E2, isotopic compositions of lavas resulting from various proportions of mixing between E1 and E2 can therefore be estimated from

$$\alpha^x_{lavas} = \gamma_E \times \alpha^x_{E1} + (1-\gamma_E) \times \alpha^x_{E2}, \quad (3.6)$$

where γ_E is the mass fraction of the normalizing isotope for the isotopic ratios α^x_{lavas}, α^x_{E1}, and α^x_{E2}.

For this mixing stage we assume a similar behaviour of trace elements during melting of the two end-members E1 and E2. In other words, most trace elements have effective partition coefficients in the two melting processes that are approximately the same.

3.2. Model solution

Here we restrict our method to systematic Sr, Nd, and Pb isotope modelling of a suite of arc lavas (such as in the Merapi case; cf. Section 5). Therefore the two-stage model developed in Section 3 leads to a system described by 16 equations. These are, for each end-member (E1 and E2), the mixing equations related to the three concentrations (Sr, Nd, and Pb) and the five isotopic ratios ($^{87}Sr/^{86}Sr$, $^{143}Nd/^{144}Nd$, $^{206}Pb/^{204}Pb$, $^{207}Pb/^{204}Pb$, and $^{208}Pb/^{204}Pb$).

3.2.1. Step-by-step calculation and Monte-Carlo approach

To solve equations of the model and thus give an estimation of the mobility and bulk solid/melt partition coefficients for Sr, Nd, and Pb in oceanic crust and sediments, we combine a step-by-step calculation with a Monte-Carlo simulation. The procedure consists of: (i) producing a large number of random values on each variable of the model, given realistic ranges of variations; (ii) using the computed values to calculate the isotopic compositions of lavas for γ_E comprised between 0 and 1 (cf. Eq. (3.6)); and (iii) comparing the obtained isotopic compositions with a true dataset (i.e., measured on natural samples), to retain or otherwise the inputted values. The calculation is repeated 1,000,000 times for statistical considerations.

3.2.2. Comparison between modelled and natural isotopic compositions

Testing the isotope compositions obtained from the Monte-Carlo simulation is done by evaluating the fit to measured data in isotope variation diagrams ($^{143}Nd/^{144}Nd$ vs. $^{87}Sr/^{86}Sr$, $^{87}Sr/^{86}Sr$ vs. $^{206}Pb/^{204}Pb$, $^{143}Nd/^{144}Nd$ vs. $^{206}Pb/^{204}Pb$, $^{207}Pb/^{204}Pb$ vs. $^{206}Pb/^{204}Pb$, and $^{208}Pb/^{204}Pb$ vs. $^{206}Pb/^{204}Pb$). For this, we calculate the distance (Dist) in a least-square sense between hyperbolae corresponding to mixing of the end-members E1 and E2 and measured data in a five dimensional space corresponding to the five isotope ratios used. However, as the level of geochemical significance is not the same for all isotopic systems (for example, $^{207}Pb/^{204}Pb$ displays weak variations due to the near extinction of ^{235}U but is measured with an analytical precision similar to that of $^{206}Pb/^{204}Pb$; therefore, treating the two ratios equally would obviously amount to overestimation of the $^{207}Pb/^{204}Pb$ information), we do not consider raw data but apply a factor designed to weigh all isotopic tracers equivalently. This weighting factor (R) is comparable in essence to that used by Allègre et al. (1986/1987) in their isotope multispace analysis, and corresponds to the ratio of the total range for the set of samples over the minimum difference between two samples above

which they are considered as significantly different (i.e., the 2σ external reproducibility of standard measurements, see Table 1).

Mathematically, the distance between modelled and measured data is given by

$$\mathrm{Dist} = \sum_{1}^{n}\left[\sum_{1}^{5}\left(\alpha_j^M - \alpha_j^C\right)^2 \times (R_j/\sigma_j)^2\right]^{(1/2)}, \quad (3.7)$$

where n is the number of samples used for comparison; α_j^M is the measure of the isotopic ratio considered ($^{87}Sr/^{86}Sr$, $^{143}Nd/^{144}Nd$, $^{206}Pb/^{204}Pb$, $^{207}Pb/^{204}Pb$ or $^{208}Pb/^{204}Pb$) and α_j^C its calculated value; σ_j is the standard deviation of the measured dataset, and R_j the weighting factor for a given isotopic ratio.

It should be noted that the distance (Dist) is not calculated, but is considered as infinite when at least one of the two end-members E1 and E2 falls within the range of variations of the measured samples.

3.2.3. Best solution

The smallest distance ($\mathrm{Dist_{min}}$) calculated among the set of 1,000,000 combinations defines the best solution; i.e., the combination of data that minimizes the difference between modelled compositions and measured data. We should, however, be aware that this best solution does not guarantee that all data will lie closely along the corresponding mixing hyperbola, thus requiring visual comparison between the hyperbola and the data in isotope variation diagrams.

A way to evaluate how reliable the best combination is is to consider the minimum distance ($D_{2\sigma}$) between measured data and the theoretical mixing curve above which they are considered as indistinguishable, i.e. within the analytical error (2σ), and to compare this distance with the calculated distance (Dist)

$$D_{2\sigma} = \sum_{1}^{n}\left[\sum_{1}^{5}(2\times\sigma_{\mathrm{ext}}^j)^2 \times (R_j/\sigma_j)^2\right]^{(1/2)}, \quad (3.8)$$

where σ_{ext}^j is the 1σ external reproducibility of the isotopic ratio considered ($^{87}Sr/^{86}Sr$, $^{143}Nd/^{144}Nd$, $^{206}Pb/^{204}Pb$, $^{207}Pb/^{204}Pb$ or $^{208}Pb/^{204}Pb$) (see also Table 1).

3.2.4. Graphic representations

Distances calculated from the combinations of inputted values other than the best solution give further information on the model. In particular comparison between results of the best solution and those obtained for the 2nd, 3rd, ..., nth smallest distances may be useful. We thus represent all combinations by using histograms of the model parameters (Fig. 3). However, we do not attribute an identical weight to all computed values of a given parameter: we attribute the ratio of the smallest total distance ($\mathrm{Dist_{min}}$) over the distance of the considered combination (Dist) as a weighting factor. This provides a weight of 1 for parameters of the best solution, and a weight inversely proportional to their distance for parameters of the other combinations (a weight of 0 is thus attributed to solutions with E1 and/or E2 falling within the range of variations of the measured samples). In other words, the less the modelled hyperbola fits the measured data, the less the corresponding parameters influence the shape of the histograms.

3.2.5. Reproducibility of the approach

To test the reproducibility of the procedure, we have twice repeated the injection of 1,000,000 randomly selected combinations (with the same ranges of variations) into the model and mixing equations. Results are illustrated in Fig. 3 in histograms of best solution-normalized parameters. The good agreement observed between the two simulations demonstrates the reproducibility of the total approach.

4. A priori variables

A total of 44 variables is used in the model (Table 2). They can be divided into three different categories: (i) 24 variables related to components; (ii) 8 variables related to

Table 1
Data normalization (Range of isotopic variations Δ, 1σ external reproducibility of standard measurements σ_{ext} and weighting factor $R = \Delta/2\sigma_{\mathrm{ext}}$ for each tracer) calculated for the Merapi medium-K and high-K lava series isotope dataset

	$^{87}Sr/^{86}Sr$	$^{143}Nd/^{144}Nd$	$^{206}Pb/^{204}Pb$	$^{207}Pb/^{204}Pb$	$^{208}Pb/^{204}Pb$
Medium-K series					
Minimum value	0.705043	0.512687	18.738	15.680	39.093
Maximum value	0.705876	0.512770	18.818	15.697	39.218
Variation (Δ)	0.000833	0.000083	0.080	0.017	0.125
σ_{ext}	0.000011	0.000012	0.003	0.003	0.008
R	39.09	3.45	11.80	2.74	8.28
High-K series					
Minimum value	0.705341	0.512676	18.737	15.676	39.084
Maximum value	0.705763	0.512782	18.768	15.696	39.158
Variation (Δ)	0.000422	0.000106	0.031	0.020	0.074
σ_{ext}	0.000011	0.000012	0.003	0.003	0.008
R	19.81	4.41	4.57	3.23	4.90

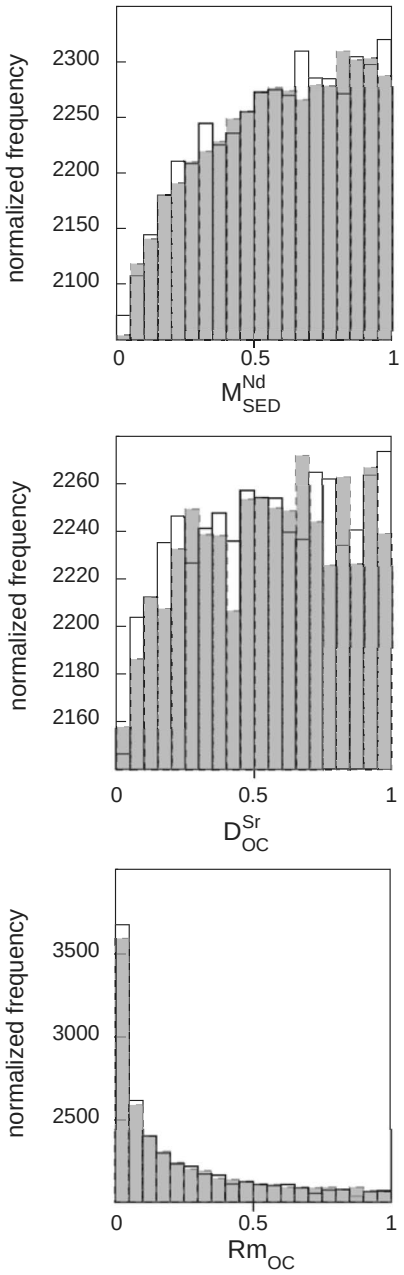

Fig. 3. Comparison of histograms of the best-solution normalized parameters M^{Nd}_{SED} (Nd mobility coefficient during sediment dehydration), D^{Sr}_{OC} (Sr bulk solid/melt partition coefficient during oceanic crust melting) and Rm_{OC} (mass ratio between melts/fluids released by subducted oceanic crust and the mantle wedge) obtained from two inputs of 1,000,000 randomly selected combinations (with the same ranges of variations) into the model equations for the medium-K series from Merapi Volcano. The good agreement observed between the two simulations demonstrates the reproducibility of the total approach.

dehydration and melting processes; and (iii) 12 variables related to behaviour of elements.

4.1. Variables related to components

These correspond to the Sr, Nd, and Pb concentrations and $^{87}Sr/^{86}Sr$, $^{143}Nd/^{144}Nd$, $^{206}Pb/^{204}Pb$, $^{207}Pb/^{204}Pb$, and $^{208}Pb/^{204}Pb$ ratios of the mantle wedge, oceanic crust and sediment components. These variables can be considered as well constrained since their values can be deduced from direct measurements of natural samples, such as Oceanic Drilling Project (ODP) samples for the oceanic crust and sediments and MORB for the mantle wedge. Note, however, that the Sr, Nd, and Pb concentrations of the mantle wedge inferred from MORB measurements have to be corrected for partial melting.

4.2. Variables related to dehydration and melting processes

These correspond to the melt fractions and dehydration rates of oceanic crust and sediments, the mass ratios between silicate melts and hydrous fluids in the H_2O-rich released phase, and the mass ratios between the released phase and the mantle wedge. While some of these variables are poorly constrained, others, including the weight fractions of hydrous fluids extracted from the slab (Peacock, 1990) and the degree of partial melting of both oceanic crust and sediments (Jonhson and Plank, 1999; Nichols et al., 1994), are known with a relatively high degree of confidence.

4.3. Variables related to behaviour of elements during slab dehydration and melting

These correspond to the respective mobility and bulk partition coefficients of Sr, Nd, and Pb in the subducted oceanic crust and sediments. These variables represent unknowns in the model. In practice, however, we assume an incompatible behaviour (i.e., a bulk partition coefficient between 0 and 1) for the three elements during melting of the two slab components.

4.4. Ranges of errors

A constant relative error of 100% is adopted for unconstrained variables (unknowns) in the model. For example, mobility and bulk partition coefficients are randomly extracted from intervals equal to 0.5 ± 0.5. Conversely, maximum errors of 10% are assumed for well-constrained variables (parameters). Among the 44 variables of the model, 28 can thus be considered as parameters and 16 as unknowns (Table 2). Therefore, the system to be solved through a step-by-step procedure comprises 16 equations for 16 unknowns.

5. Case study: Merapi volcano, Java island, Sunda arc

In the following sections, we apply parts of the simplified model of arc-lava genesis described above to a new set of Sr, Nd, and Pb isotope data on volcanics from Merapi volcano. The point of this application is to emphasize the different aspects of our approach and examine values of the parameters (for example, bulk partition coefficients, mobility coefficients, and slab-derived melt/fluid ratios)

Table 2
List of the variables used in the model

Variable		Mean value	Variation	% error
MW^{87}	$^{87}Sr/^{86}Sr$ of mantle wedge	0.702925	0.000095	0.014
MW^{143}	$^{143}Nd/^{144}Nd$ of mantle wedge	0.513070	0.000013	0.003
MW^{206}	$^{206}Pb/^{204}Pb$ of mantle wedge	17.923	0.038	0.21
MW^{207}	$^{206}Pb/^{204}Pb$ of mantle wedge	15.488	0.021	0.13
MW^{208}	$^{206}Pb/^{204}Pb$ of mantle wedge	37.776	0.05	0.13
MW^{Sr}	Sr concentration of mantle wedge	15.0	1.5	10
MW^{Nd}	Nd concentration of mantle wedge	1.0	0.1	10
MW^{Pb}	Pb concentration of mantle wedge	0.065	0.006	9.23
OC^{87}	$^{87}Sr/^{86}Sr$ of subducted oceanic crust	0.703450	0.000753	0.11
OC^{143}	$^{143}Nd/^{144}Nd$ of subducted oceanic crust	0.512949	0.000094	0.02
OC^{206}	$^{206}Pb/^{204}Pb$ of subducted oceanic crust	18.610	0.560	3.01
OC^{207}	$^{207}Pb/^{204}Pb$ of subducted oceanic crust	15.576	0.085	0.54
OC^{208}	$^{208}Pb/^{204}Pb$ of subducted oceanic crust	38.645	0.685	1.77
OC^{Sr}	Sr concentration of subducted oceanic crust	125.0	12.5	10
OC^{Nd}	Nd concentration of subducted oceanic crust	11.0	1.1	10
OC^{Pb}	Pb concentration of subducted oceanic crust	0.2	0.02	10
SED^{87}	$^{87}Sr/^{86}Sr$ of subducted sediments	0.711348	0.005472	0.77
SED^{143}	$^{143}Nd/^{144}Nd$ of subducted sediments	0.512391	0.000286	0.05
SED^{206}	$^{206}Pb/^{204}Pb$ of subducted sediments	18.904	0.086	0.45
SED^{207}	$^{207}Pb/^{204}Pb$ of subducted sediments	15.719	0.022	0.14
SED^{208}	$^{208}Pb/^{204}Pb$ of subducted sediments	39.273	0.055	0.14
SED^{Sr}	Sr concentration of subducted sediments	220.0	22	10
SED^{Nd}	Nd concentration of subducted sediments	33.0	3.3	10
SED^{Pb}	Pb concentration of subducted sediments	25.0	2.5	10
M^{Sr}_{OC}	Mobility of Sr in subducted oceanic crust	0.5	0.5	100
M^{Nd}_{OC}	Mobility of Nd in subducted oceanic crust	0.5	0.5	100
M^{Pb}_{OC}	Mobility of Pb in subducted oceanic crust	0.5	0.5	100
D^{Sr}_{OC}	Partition coefficient of Sr in subducted oceanic crust	0.5	0.5	100
D^{Nd}_{OC}	Partition coefficient of Nd in subducted oceanic crust	0.5	0.5	100
D^{Pb}_{OC}	Partition coefficient of Pb in subducted oceanic crust	0.5	0.5	100
M^{Sr}_{SED}	Mobility of Sr in subducted sediments	0.5	0.5	100
M^{Nd}_{SED}	Mobility of Nd in subducted sediments	0.5	0.5	100
M^{Pb}_{SED}	Mobility of Pb in subducted sediments	0.5	0.5	100
D^{Sr}_{SED}	Partition coefficient of Sr in subducted sediments	0.5	0.5	100
D^{Nd}_{SED}	Partition coefficient of Nd in subducted sediments	0.5	0.5	100
D^{Pb}_{SED}	partition coefficient of Pb in subducted sediments	0.5	0.5	100
Rm_{OC}	Mass of fluids released by subducted oceanic crust/ mass of mantle wedge	0.5	0.5	100
Rm_{SED}	Mass of fluids released by subducted sediments/ mass of mantle wedge	0.5	0.5	100
f_{OC}	Dehydration rate of subducted oceanic crust	0.015	0.0015	10
f_{SED}	Dehydration rate of subducted sediments	0.015	0.0015	10
F_{OC}	Partial melting degree of subducted oceanic crust	0.15	0.015	10
F_{SED}	Partial melting degree of subducted sediments	0.015	0.0015	10
$\frac{Tm_{OC}}{Tm_{OC}+1}$	Tm_{OC} = mass of melts/mass of hydrated fluids from subducted oceanic crust	0.5	0.5	100
$\frac{Tm_{SED}}{Tm_{SED}+1}$	Tm_{SED} = mass of melts/mass of hydrated fluids from subducted sediments	0.5	0.5	100

Data source: Mantle wedge, Dosso et al. (1988); oceanic crust, Weis and Frey (1996); sediments, Ben Othman et al. (1989); Plank and Langmuir (1998); Hemming and McLennan (2001).

that can account for the isotopic arrays found in arc volcanoes.

5.1. Geological setting

Merapi volcano has been built up in the central part of Java island over the last 650 ± 250 kyr (Camus et al., 2000). Its activity, related to the northward subduction of the Indo-Australian plate beneath the Eurasian plate (Hamilton, 1979; Turner and Foden, 2001), is characterized by semi-continuous lava extrusions producing summit domes and periodic collapse events triggering pyroclastic flows (Camus et al., 2000). Although an overall isotopic trend has been documented for Merapi volcanics (e.g., Gertisser and Keller, 2003a), three distinct components are generally considered for their source. These are the mantle wedge, the subducted oceanic crust and its sediment cover (McDermott and Hawkesworth, 1991; Alves et al., 1999; Turner and Foden, 2001; Gertisser and Keller, 2003a). In addition, even though a slight role for shallow-level crustal contamination has been envisioned (Turner and Foden, 2001; Chadwick et al., 2005), this process has not significantly changed the isotopic characteristics of erupted whole rocks in the region (Alves et al., 1999; Gertisser and Keller, 2003a) and thus it will not be considered in the following discussion.

5.2. Major and isotope analyses

5.2.1. Analytical procedures

All samples were coarse-crushed in a hydraulic piston crusher before being reduced to powder in an agate shatterbox. Major-element concentrations were measured by ICP-AES, at the Service d'Analyse des Roches et des Minéraux (SARM, CRPG/Nancy) with a precision better than 1% except for MnO, CaO, and Na_2O (<2%) and TiO_2 and P_2O_5 (<5%). Standards and reproducibilities can be downloaded from the SARM website at http://www.crpg.cnrs-nancy.fr/SARM.

Sr isotope ratios were measured by TIMS at the Pacific Centre for Isotopic and Geochemical Research (PCIGR/Vancouver), whereas isotopic composition measurements of Nd and Pb were made by MC-ICP-MS at the Université Libre de Bruxelles (ULB). Sr, Nd, and Pb were separated using the chemical procedure described in Weis and Frey (1991) and Weis et al. (2005). Prior to dissolution, samples were leached several times during a 15 mn period with 6N HCl in an ultrasonic bath to remove any secondary contamination. The mean weight loss during leaching was 34%. Total blank values were negligible (< 1 ng) for each element with respect to sample abundances (> 60,000, 200, and 3000 ng for Sr, Pb, and Nd, respectively).

Sr was measured dynamically and corrected for mass discrimination to $^{86}Sr/^{88}Sr = 0.1194$. Seven analyses of the SRM987 NIST standard performed during the course of the study give a mean $^{87}Sr/^{86}Sr$ value of 0.710247 ± 24 (2σ). The total external reproducibility based on measurements of replicates (crushing, chemical separation, and mass spectrometric run, cf. samples MP 231 a and b and MP 304 a and b) is better than 30 ppm.

Nd was measured dynamically and corrected for potential Ce and Sm interferences by monitoring ^{140}Ce and ^{147}Sm, respectively. Mass discrimination was normalized to $^{146}Nd/^{144}Nd = 0.7219$. The $^{143}Nd/^{144}Nd$ mean value obtained for the Rennes standard (Chauvel and Blichert-Toft, 2001), analysed every two samples, was 0.511927 ± 24 (2σ, $n = 16$). The total external reproducibility based on the replicate sample analyses (crushing, chemical separation, and mass spectrometric run) is better than 47 ppm.

Pb isotope measurements were made statically. Mass discrimination was corrected for by using the Tl doping technique, assuming the same fractionation effect between Tl and Pb and $^{203}Tl/^{205}Tl = 2.3885$ (Weis et al., 2005). Isobaric interference between ^{204}Hg and ^{204}Pb was controlled by monitoring ^{202}Hg. Repeated analyses ($n = 28$) of the SRM981 NIST standard (200 ppb Pb diluted with 50 ppb Tl in 0.05 M HNO_3), measured every two samples, give mean values of 16.941 ± 6 (2σ), 15.497 ± 6 (2σ) and 37.717 ± 15 (2σ) for $^{206}Pb/^{204}Pb$, $^{207}Pb/^{204}Pb$, and $^{208}Pb/^{204}Pb$, respectively. The total external reproducibility based on the replicate sample analyses (crushing, chemical separation, and mass spectrometric run) is better than 400 ppm.

5.2.2. Major-element and isotope results

Twenty samples (see Berthommier (1990) for locations) were analyzed in this study. They all have SiO_2 contents between 48 and 55% wt, MgO between 2.5 and 4.8% wt, and ($Na_2O + K_2O$) between 3.7 and 5.8% wt (Table 3 and Fig. 4); they correspond to basalts, basaltic andesites, trachybasalts, and basaltic trachyandesites. The 20 samples span the period between 400 kyr ago and recent flows. Consequently, Sr, Nd, and Pb isotopic compositions were not corrected for radioactive decay of Rb, Sm, U, and Th. Isotope data are given in Table 4 and illustrated in Fig. 5. They are in agreement for Sr and Nd isotopes with

Table 3
Major-element concentrations for samples from Merapi volcano

	Series	SiO_2	Al_2O_3	Fe_2O_3	MnO	MgO	CaO	Na_2O	K_2O	TiO_2	P_2O_5	LOI	Total
MP 1	MK	53.6	19.0	8.36	0.18	2.67	8.77	3.41	2.05	0.77	0.32	0.74	99.87
MP 14	MK	53.7	19.1	8.66	0.17	3.15	9.01	3.33	1.54	0.78	0.26	0.21	99.91
MP 21	MK	48.3	19.9	10.40	0.16	3.77	10.30	2.68	1.00	1.01	0.27	2.10	99.89
MP 29	HK	52.0	19.0	9.36	0.18	3.65	9.27	3.21	1.63	0.86	0.27	0.48	99.91
MP 41	HK	54.1	18.6	8.59	0.19	2.75	7.99	3.60	1.81	0.83	0.28	1.15	99.89
MP 42	HK	54.3	18.7	8.18	0.18	2.73	8.43	3.71	1.87	0.83	0.29	0.59	99.81
MP 43	MK	55.3	18.7	8.18	0.16	2.76	8.39	3.50	1.76	0.85	0.27	−0.02	99.87
MP 63	MK	48.5	19.6	10.60	0.19	4.82	9.16	2.70	1.15	0.90	0.25	2.21	100.08
MP 65	MK	49.7	19.3	10.80	0.16	3.17	9.28	2.82	1.91	1.00	0.28	1.55	99.97
MP 84-g	HK	55.2	19.5	7.82	0.19	2.47	8.52	3.68	2.15	0.73	0.29	−0.21	100.55
MP 84-1	HK	54.9	19.2	7.82	0.19	2.50	8.52	3.65	2.12	0.73	0.30	−0.03	99.93
MP 88	MK	55.1	18.7	7.91	0.18	2.65	8.25	3.56	1.86	0.83	0.27	0.33	99.64
MP 93	MK	55.2	19.0	7.10	0.17	2.68	7.61	3.32	1.57	0.62	0.22	2.39	99.88
MP 231	MK	49.1	20.1	9.36	0.15	3.94	10.80	2.87	1.25	0.79	0.21	1.68	100.25
MP 232	MK	49.3	19.2	10.00	0.15	4.51	10.20	2.93	1.44	0.86	0.24	1.14	99.97
MP 243	MK	52.7	18.3	9.15	0.20	4.00	9.01	2.98	1.40	0.84	NA	NA	98.58
MP 288	MK	54.1	18.8	8.73	0.17	3.46	8.74	3.44	1.75	0.90	0.29	−0.02	100.38
MP 297	HK	51.6	18.4	9.44	0.21	4.06	9.75	3.30	1.80	0.94	NA	NA	99.50
MP 304	HK	52.4	19.2	9.26	0.19	3.53	9.42	3.37	2.07	0.89	0.27	−0.19	100.60
MP 305	HK	52.2	19.0	9.23	0.18	3.51	9.40	3.33	2.09	0.87	0.24	−0.15	100.05
MP 307	MK	54.6	19.2	8.27	0.19	2.84	8.64	3.56	1.71	0.79	0.27	−0.07	100.07

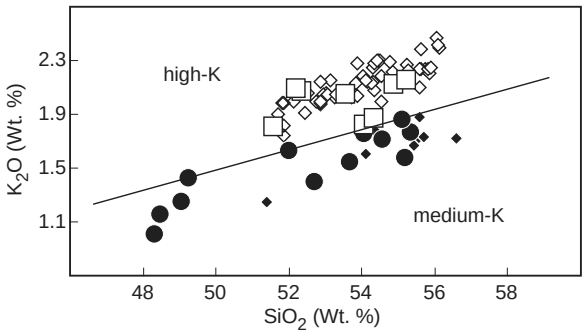

Fig. 4. Plot of K_2O vs. SiO_2 for Merapi lavas. Black symbols correspond to the medium-K lava series (circles: this study; diamonds: Gertisser and Keller, 2003a,b). White symbols are for the high-K lava series (squares: this study; diamonds: Gertisser and Keller, 2003a,b). Classification after Le Maitre et al. (1989).

previous values for lavas from Merapi volcano (McDermott and Hawkesworth, 1991; Turner and Foden, 2001; Gertisser and Keller, 2003a), but they extend towards more radiogenic $^{206}Pb/^{204}Pb$ values than those previously reported by Gertisser and Keller (2003a). Although the samples display a small range of variations ($^{87}Sr/^{86}Sr = 0.705043$–$0.705876$, $^{143}Nd/^{144}Nd = 0.512676$–$0.512782$, $^{206}Pb/^{204}Pb = 18.7374$–$18.8180$, $^{207}Pb/^{204}Pb = 15.6760$–$15.6975$, $^{208}Pb/^{204}Pb = 39.0845$–$39.2176$) relative to the entire range displayed by arc lavas, overall they define clear isotopic trends on variation diagrams. More precisely, the data define two sub-parallel trends (Fig. 5C), which correspond to the Medium-K (basalts and basaltic andesites) and High-K (trachybasalts and basaltic trachyandesites) series of Gertisser and Keller (2003a) (see also Fig. 4). These authors have proposed that this distinction is inherited from the primary parental magmas and clearly reflects a property of the mantle sources, such as variable contribution of subducted sediments, rather than the product of high-level differentiation or contamination processes.

Below we will consider the two series separately. First, we apply our method to the medium-K series, because it has a greater number of data, defines clear binary mixing relationships and is thus better suited for petrogenetic modelling. We then consider the high-K series for comparison.

5.3. Range of variations of variables

The 44 variables used in the model are listed in Table 2, together with their ranges of variations.

5.3.1. Variables related to the mantle wedge, oceanic crust, and sediment components

Sr, Nd, and Pb isotopic compositions of the mantle wedge beneath Merapi volcano are obtained from a set of MORB samples from the South East Indian Ridge (SEIR; Dosso et al., 1988), the nearest ridge to the Indonesian Arc, away from the influence of the Kerguelen and Amsterdam/St. Paul hotspots. The Sr, Nd, and Pb concentrations of the mantle wedge are also estimated from the SEIR MORB, after removing the effect of partial melting using a batch melting process with a melt fraction of 10% (Klein and Langmuir, 1987; Hofmann, 1988; Schiano et al., 1993). Isotopic ratios and concentrations for the oceanic crust and sediments are taken from the mean values for samples collected during the Ocean Drilling Project (ODP) in the Wharton Basin (Weis and Frey, 1996) and in the Indian Ocean (100°–120°E and 0°–20°S; see

Table 4
Strontium, neodymium, and lead isotope data for samples from Merapi volcano

	$^{87}S/^{86}Sr \pm 2\sigma_m$	$^{143}Nd/^{144}Nd \pm 2\sigma_m$	$^{206}Pb/^{204}Pb \pm 2\sigma_m$	$^{207}Pb/^{204}Pb \pm 2\sigma_m$	$^{208}Pb/^{204}Pb \pm 2\sigma_m$
MP1	0.705763 ± 6	0.512726 ± 10	18.7677 ± 7	15.6907 ± 6	39.1519 ± 34
MP 14	0.705156 ± 5	0.512735 ± 10	18.7513 ± 6	15.6805 ± 6	39.1078 ± 40
MP 21	0.705435 ± 8	0.512747 ± 9	18.8099 ± 7	15.6969 ± 8	39.2105 ± 32
MP 29	0.705531 ± 3	0.512724 ± 14	18.7858 ± 6	15.6910 ± 5	39.1684 ± 38
MP 41	0.705356 ± 5	0.512769 ± 8	18.7408 ± 7	15.6760 ± 7	39.0845 ± 34
MP 42	0.705341 ± 7	0.512782 ± 10	18.7374 ± 7	15.6778 ± 7	39.0906 ± 41
MP 43	0.705221 ± 5	0.512764 ± 12	18.7595 ± 10	15.6847 ± 9	39.1257 ± 46
MP 63	0.705480 ± 7	0.512741 ± 13	18.7921 ± 8	15.6908 ± 9	39.1682 ± 30
MP 84-g	0.705748 ± 7	0.512713 ± 12	18.7592 ± 7	15.6835 ± 6	39.1214 ± 24
MP 84-1	0.705755 ± 4	0.512700 ± 9	18.7601 ± 18	15.6849 ± 23	39.1341 ± 73
MP 88	0.705179 ± 5	0.512757 ± 9	18.7544 ± 7	15.6843 ± 7	39.1224 ± 22
MP 93	0.705115 ± 5	0.512770 ± 7	18.7570 ± 6	15.6840 ± 6	39.1172 ± 43
MP 231 a	0.705816 ± 6	0.512727 ± 13	18.8180 ± 9	15.6972 ± 9	39.2165 ± 61
MP 231 b	0.705821 ± 6	0.512706 ± 16	18.8110 ± 28	15.6937 ± 27	39.2008 ± 81
MP 232	0.705876 ± 6	0.512687 ± 20	18.8183 ± 6	15.6975 ± 5	39.2176 ± 22
MP 243	0.705128 ± 9	0.512769 ± 9	18.7606 ± 9	15.6881 ± 8	39.1332 ± 24
MP 288	0.705043 ± 5	0.512750 ± 10	18.7383 ± 9	15.6813 ± 11	39.0935 ± 34
MP 297	0.705647 ± 6	0.512676 ± 10	18.7467 ± 15	15.6787 ± 13	39.1015 ± 38
MP 304 a	0.705688 ± 4	0.512704 ± 13	18.7674 ± 10	15.6960 ± 11	39.1579 ± 38
MP 304 b	0.705667 ± 5	0.512710 ± 12	18.7613 ± 15	15.6910 ± 13	39.1440 ± 43
MP 305	0.705646 ± 3	0.512693 ± 13	18.7563 ± 13	15.6854 ± 14	39.1231 ± 48
MP 307	0.705411 ± 7	0.512745 ± 9	18.7756 ± 5	15.6886 ± 5	39.1518 ± 20

$2\sigma_m$ is the internal reproducibility. Duplicate analyses are indicated by letters a and b.

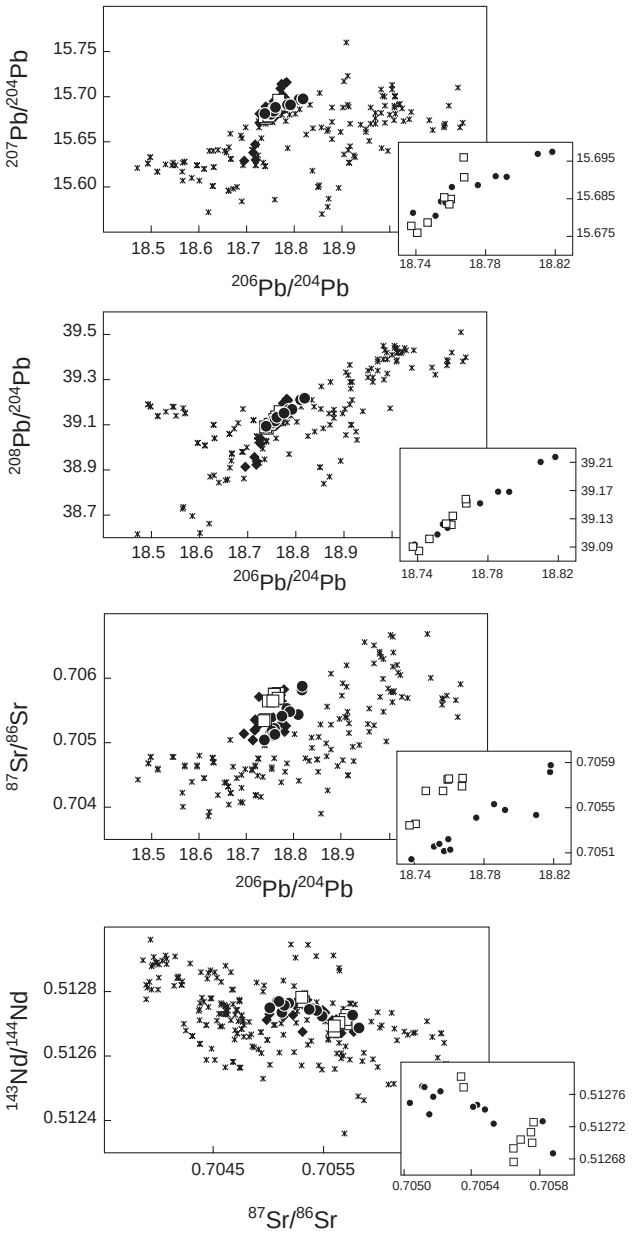

Fig. 5. $^{207}Pb/^{204}Pb$ vs. $^{206}Pb/^{204}Pb$, $^{208}Pb/^{204}Pb$ vs. $^{206}Pb/^{204}Pb$, $^{87}Sr/^{86}Sr$ vs. $^{206}Pb/^{204}Pb$ and $^{143}Nd/^{144}Nd$ vs. $^{87}Sr/^{86}Sr$ for Merapi lavas. Black circles: medium-K series from Merapi (this study); squares: high-K series from Merapi (this study); black diamonds: Merapi lavas (Gertisser and Keller, 2003a); crosses: Sunda arc lavas (Edwards et al., 1991, 1993, 1994; Gerbe et al., 1992 ; Gill and Williams, 1990; Hoogewerff et al., 1997; McDermott and Hawkesworth, 1991; Stolz et al., 1990; Turner and Foden, 2001; Turner et al., 2003; Varekamp et al., 1989; Varne and Foden, 1986; Woodhead et al., 2001).

compilation in Ben Othman et al., 1989; Plank and Langmuir, 1998; Hemming and McLennan, 2001), respectively.

The sample populations used to estimate the mean isotopic values of the components show relatively small variations in $^{87}Sr/^{86}Sr$, $^{143}Nd/^{144}Nd$, $^{206}Pb/^{204}Pb$, $^{207}Pb/^{204}Pb$, and $^{208}Pb/^{204}Pb$ ratios. We thus consider the ranges of variations of these populations as ranges of errors of the parameters. Practically, values of the 5 isotopic ratios are randomly computed, independently from each other. For sediments, however, this procedure cannot be carried out because clear binary relationships are observed between the different isotopic tracers (cf. Ben Othman et al., 1989; Plank and Langmuir, 1998; Hemming and McLennan, 2001). As an alternative, we randomly select a $^{206}Pb/^{204}Pb$ value and then we re-calculate the ranges of variations from which $^{87}Sr/^{86}Sr$, $^{143}Nd/^{144}Nd$, $^{207}Pb/^{204}Pb$, and $^{208}Pb/^{204}Pb$ ratios can be extracted, using the correlations in isotopic diagrams.

For trace-element concentrations of the components we use an arbitrary range of errors of 10%.

5.3.2. Variables related to dehydration and melting processes

For subducted sediments, an average degree of partial melting of 15% is assumed based on the experiments of Jonhson and Plank (1999). Nichols et al. (1994) have shown that the melt productivity (i.e., the amount of melt for a given ΔT) for sediments is much higher than for oceanic crustal material. Accordingly, we postulate a factor of 10 between the average melting degrees of the two slab components. Coupled with the fact that the melt fractions are parameters (i.e., well-constrained variables with errors of 10%) of the model, partial melting degrees of $1.50 \pm 0.15\%$ and $15.0 \pm 0.5\%$ are thus chosen for the oceanic crust and sediments, respectively.

Based on the studies of Peacock (1990) and Tatsumi and Kogiso (1997), values of $1.50 \pm 0.15\%$ (10% relative error) for weight fractions of hydrous fluids extracted from both down-going oceanic crust and sediments are considered plausible and are used in subsequent modelling. In contrast, there is, to our knowledge, no estimate of the mass ratios (Tm_{OC} and Tm_{SED}, see Table 2) between melts and fluids released from the oceanic crust and sediments in the literature. Thus we consider Tm values between 0 and $+\infty$. Practically, we define the $Tm/(Tm+1)$ ratio and set its range of variations between 0 and 1 (0.5 ± 0.5, 100% relative error) for both the oceanic crust and sediments. Finally, a value of 1 ($Rm = 0.5 \pm 0.5$; 100% relative error) represents a reasonable upper limit for mass ratios Rm_{OC} and Rm_{SED} between the slab component-derived melts/fluids and the mantle wedge. Note that Tm_{OC}, Tm_{SED}, Rm_{OC}, and Rm_{SED} correspond to unknowns in the model.

5.3.3. Variables related to behaviour of elements

Bulk solid/melt partition and mobility coefficients for Sr, Nd, and Pb during melting and dehydration of oceanic crust and sedimentary materials also represent unknowns (100% relative errors) of the model. However, it seems realistic to suppose that Sr, Nd, and Pb behave as incompatible elements during partial melting of the subducted components. A value of 0.5 ± 0.5 is thus attributed to all bulk partition and mobility coefficients.

6. Discussion

In this section, we evaluate the results of our modelling of the medium-K lava series from Merapi volcano.

First, we consider values of the parameters obtained for the best solution. The whole set of random combinations is then assessed through examination of histograms of the model parameters. Finally, we compare the results with those obtained for the high-K lava series from Merapi volcano.

6.1. The best solution

The Dist value for the best solution of our modelling (i.e., the solution that minimizes the distance between measured data and the computed mixing hyperbola, see Section 3.2.2 and Eq. (3.7)) is $<2\sigma$ (i.e., $<D_{2\sigma}$). The corresponding

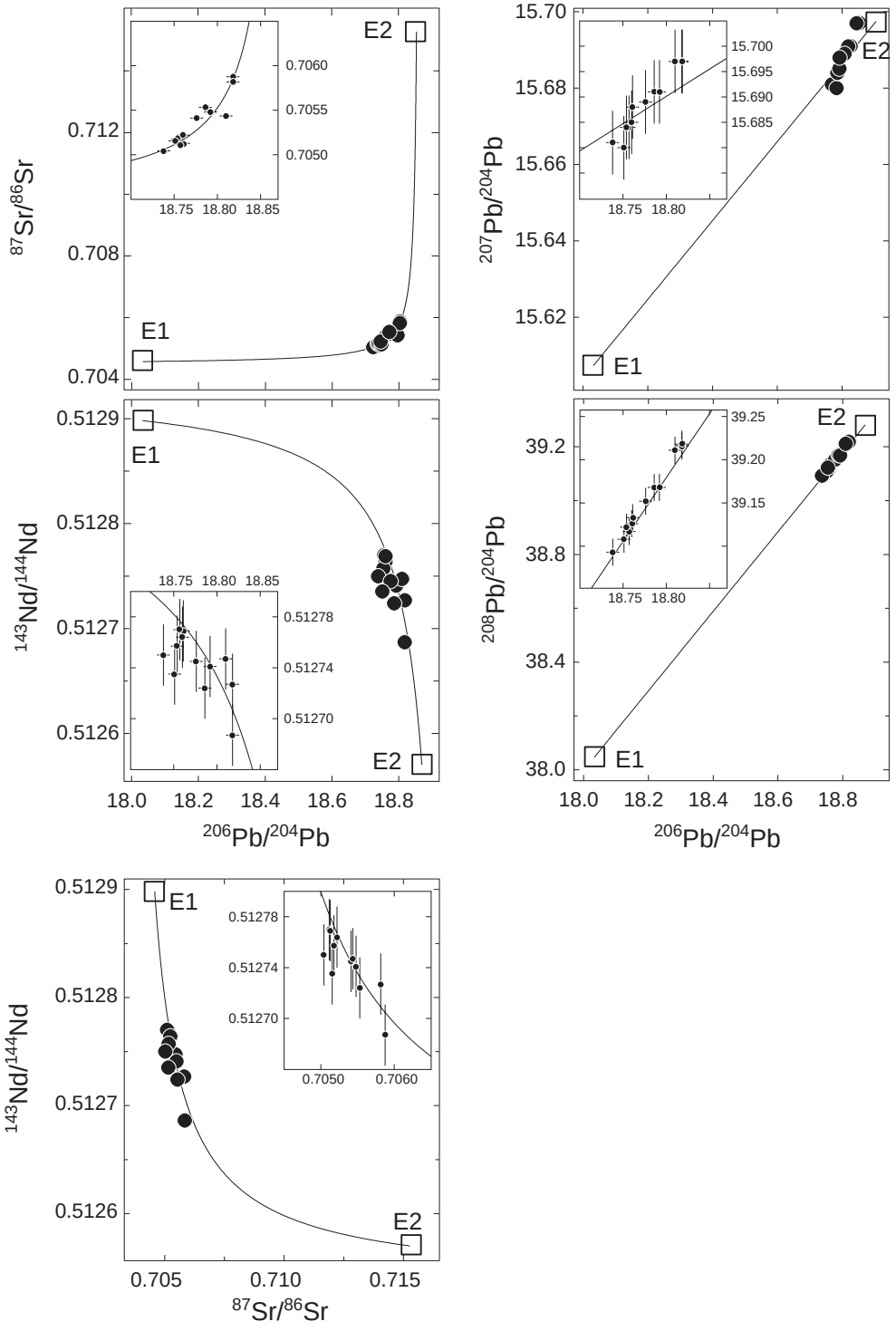

Fig. 6. Isotope diagrams comparing the mixing hyperbola computed for the best solution of our modelling in five-dimensional isotopic space with data for the medium-K lava series from Merapi volcano. Inserts show the error bars (2σ).

mixing hyperbola between the two end-members E1 and E2 generated in the first stage of the model (metasomatism of the mantle wedge by H_2O-rich phases released from the subducted oceanic crust and sediments) is reported in Fig. 6, together with isotopic data for the medium-K series. The good agreement observed between the calculated curve and the data gives additional support to our assumption that isotopic compositions of the medium-K lava series from Merapi volcano define a pseudo-binary mixing line formed by mixing three distinct components in a multi-stage process. Furthermore, it should be noted that direct binary mixing of the involved components (given the same isotopic and elemental characteristics of the best solution of our model) cannot account for the data (Fig. 7).

Values of the unknowns for the best solution of the model are displayed in Figs. 8A–C (in grey). They include (i) mobility (M^x) and bulk solid/melt partition (D^x) coefficients for Sr, Nd, and Pb in the subducted oceanic crust and sediments (i.e., the behaviour parameters during dehydration and melting processes); and (ii) melt/fluid mass ratios (Tm) in the slab-derived hydrous phase and the mass ratio (Rm) between this released phase and the mantle wedge (i.e., the proportions of the involved parts).

From Figs. 8A–C, several features of the best solution are immediately apparent. First, the inferred mobility coefficients for Sr, Nd, and Pb during sediment dehydration are relatively high, $\geqslant 50\%$. This challenges experimental studies that suggest low mobility coefficients ($<20\%$) for Sr and Nd (Aizawa et al., 1999). In contrast, during dehydration of the oceanic crust, the inferred mobility coefficient for the REE Nd is very low relative to those for Sr and Pb, as already noted by Tatsumi and Kogiso (1997). But in our case, Sr is more mobile than Pb, contrary to the observations of Tatsumi and Kogiso (1997). Second, highly contrasted Sr–Nd–Pb incompatibility orders are obtained during melting of the slab components; the order of trace-element incompatibility is $D_{Nd} \leqslant D_{Sr} < D_{Pb}$ during sediment melting and $D_{Sr} < D_{Pb} \approx D_{Nd}$ during oceanic crust melting. This is a clear indication of distinct proportions of the residual phases in the two components or of the presence of distinct residual phases. Note also that a comparable behaviour between LREE (Ce, Nd) and Pb during partial melting of oceanic crust is in agreement with the bulk partition coefficients during the generation of MORB (Hofmann, 1997). A third feature is the minor role for the mantle wedge relative to the slab-derived melt/fluid phase, as indicated by the Rm_{OC} and Rm_{SED} ratios >0.8. Also there is a significant difference in the ratios between melts and fluids released from the subducted oceanic crust ($Tm_{OC}/(Tm_{OC}+1)$ ~ 0.3) and sediments ($Tm_{SED}/(Tm_{SED}+1)$ ~ 0.7). The metasomatic phase issued from the oceanic crust is thus more hydrous than that from the sediments, in agreement with the lower melting temperature for sediments (Nichols et al., 1994).

6.2. Histograms of the model parameters

The entire set of 1,000,000 combinations, represented as histograms of the model parameters weighted by the $Dist_{min}/Dist$ ratio (see Section 3.2.4), is also shown in Figs. 8A–C. A high peak in these histograms could reflect a small number of solutions with a high weighting (i.e., that fit the data well), or a large number of solutions with a small weighting. The former hypothesis is supported by the fact that the weighted histograms and raw histograms of combinations with $Dist < 1.5 \times D_{2\sigma}$ (115 combinations) have comparable shapes (Fig. 9).

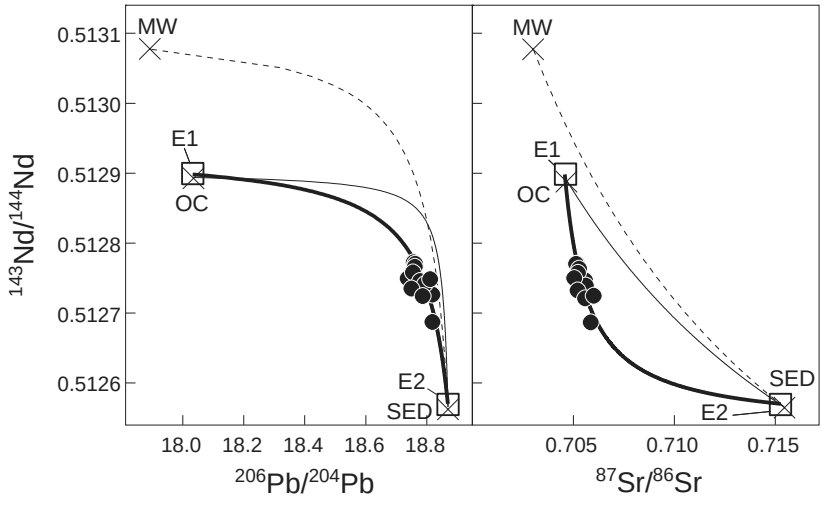

Fig. 7. Plots of $^{143}Nd/^{144}Nd$ vs. $^{206}Pb/^{204}Pb$ and $^{87}Sr/^{86}Sr$ comparing pseudo-binary mixing hyperbola computed for the best solution of the medium-K lava series modelling and direct binary mixing of the three involved components (mantle wedge, MW; subducted oceanic crust, OC; and subducted sediments, SED) having the isotopic and elemental characteristics of the best solution. Medium-K lava series: black circles; end-members (E1 and E2): squares; components: crosses; mixing between E1 and E2: thick black line; mixing between OC and SED: thin line; mixing between MW and SED: dashed line.

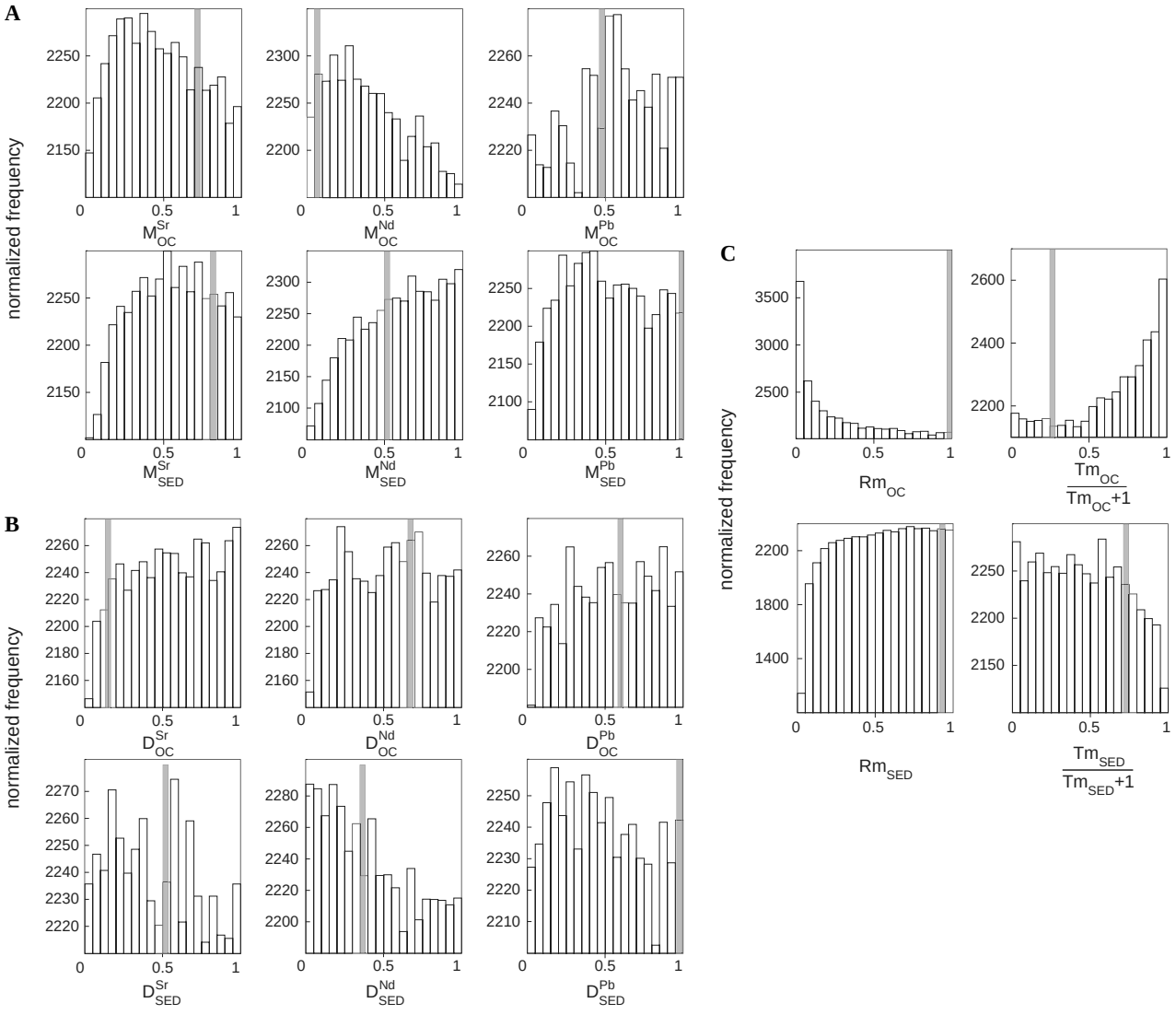

Fig. 8. Histograms of the best-solution normalized model parameters obtained for the Merapi medium-K lava series modelling. (A) Mobility (M^x); (B) bulk solid/melt partition (D^x) coefficients for Sr, Nd, and Pb in the subducted oceanic crust and sediments; (C) Melt/fluid mass ratios (Tm) in the slab-derived hydrous phase and mass ratio (Rm) between this released phase and the mantle wedge. Also shown in grey are the values of the parameters for the best solution of the model.

Although many histograms of the model parameters do not show a "single-peaked" distribution, they generally allow identification of a predominant value or range of values. For example, a maximum peak around 20% is clearly discernible for the Nd mobility coefficient M^{Nd}_{OC} during oceanic crust dehydration (Fig. 8A). Conversely, mass ratios between melts/fluids released by subducted sediments and the mantle wedge (Rm_{SED}) display an almost flat distribution between 10 and 100% (Fig. 8C). This is a clear indication that contrary to M^{Nd}_{OC}, Rm_{SED} values do not greatly influence calculation of our model of arc-lava genesis nor, consequently mixing hyperbolae between end-members E1 and E2. Identification of the predominant values leads to the characterization of the most appropriate average combination. An important feature of this average combination is the change in Sr, Nd and Pb behaviour during dehydration of the two subducted components; during oceanic crust dehydration the mobility sequence is $M^{Nd}_{OC} \approx M^{Sr}_{OC} < M^{Pb}_{OC}$, whereas $M^{Pb}_{SED} < M^{Sr}_{SED} < M^{Nd}_{SED}$ during sediment dehydration. In contrast, histograms for Sr, Nd, and Pb bulk solid/melt partition coefficients show small-scale fluctuations that preclude identification of any predominant value, except for the D^{Nd}_{SED} and D^{Pb}_{SED} histograms which suggest an incompatible behaviour of Nd and Pb during sediment melting. Significantly, Rm and Tm mass ratios determined for the average combination distinguish oceanic crust from sediments. Maximum values observed for Rm_{OC} (<10%) and Rm_{SED} (between 10 and 100%) highlight a major contribution of down-going sediments to the metasomatizing phase, and comparison between Tm_{OC} and Tm_{SED} histograms emphasizes the hydrous character of the oceanic crust-derived phase relative

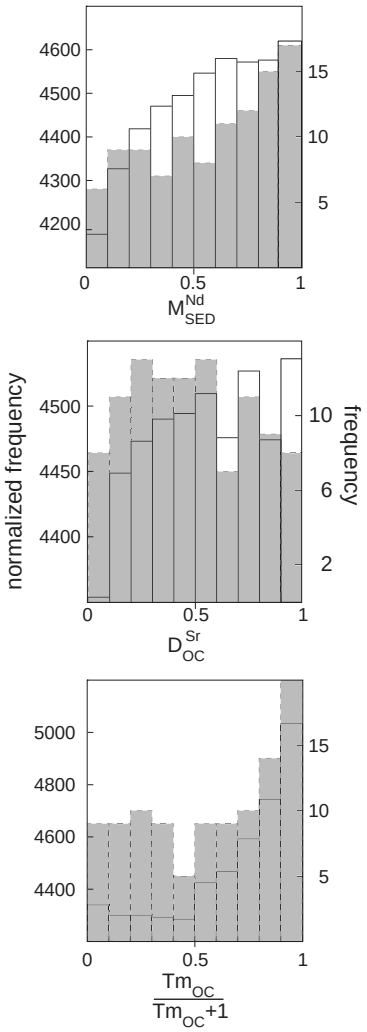

Fig. 9. Comparison of the best-solution normalized histograms of model parameters shown in Fig. 8 (left *Y*-axis) with the raw histograms (grey; right *Y*-axis) of the combinations having a total distance between modelled mixing hyperbolae and measured data less than $1.5\times\ D_{2\sigma}$ (115 combinations).

to that released from sediments. It should also be noted that, although the amount of the oceanic-crust derived phase is subordinate to that from sediments, its value is precisely characterized, indicating that Rm_{OC} acts as a major parameter of our model.

An additional important observation to be made is that the oceanic crust and sediments show well-defined, but complementary, *Rm* and *Tm* histograms (Fig. 8C). In this context, the absence of precise constraints on most of the mobility and bulk partition coefficients demonstrates that our two-stage procedure for isotope modelling of a cogenetic suite of arc lavas is more controlled by the involved components (mantle wedge, oceanic crust, sediments and their derivatives) than the various processes (dehydration, melting, and mixing).

It should be noted that, while the majority of the principal values defining the average combination are consistent with values of the best solution, some show significant differences, for example the Sr, Nd, and Pb mobility coefficients during oceanic crust and sediment dehydration and the mass ratio between melt and fluid from the oceanic crust. The differences illustrate the fact that a combination cannot provide a unique solution for the model. Several combinations of inputted values can account for the same arc lava data. These combinations do not differ in just one variable, but in all of them; i.e., any modification of an unconstrained variable (unknown) would induce some change in all the others. In the Merapi lava suites unknowns in the model relate to the melting and dehydration processes (see Section 5.3). This suggests that the two processes are closely related and influence each other, in agreement with previous studies that suggest a correlation between the degree of melting in arc settings and the amount of H_2O in the source (Stolper and Newman, 1994).

Such a balancing mechanism can also occur at the scale of the parameters of one process only. For example a decreasing degree of partial melting is balanced by a decrease in the computed bulk solid/melt partition coefficients (i.e., elements are more incompatible). Similarly, a lower mobility coefficient for an element results in a higher dehydration rate. As a consequence of these associations there is no simple relationship between unconstrained variables of our model. This is illustrated by the absence of binary correlations between these variables, when the 115 combinations with Dist $< 1.5\times D_{2\sigma}$ used to construct raw histograms of Fig. 9 are considered.

6.3. Origin of the high-K lava series from Merapi volcano

According to Gertisser and Keller (2003a), the distinction between high-K and medium-K lava series in Merapi is primary and reflects a variable contribution of subducted sediments in their mantle sources, rather than shallow-level processes. To illustrate this hypothesis, and as an independent test of our procedure, we applied a simplified version of the modelling to the data of the high-K lava series. We adopted a calculation in which the inputted values of the variables are assumed to be identical to those found for the best solution of the medium-K lava series modelling, except for the sediment-related variables (isotope ratios and trace-element concentrations) which are randomly produced. Then the step-by-step calculation and Monte-Carlo simulation of the procedure led to the characterization of the new end-member E2 and mixing hyperbola between E1 and E2. Again, a best solution can be defined, which minimizes the distance between modelled compositions and the high-K lava data. Fig. 10 shows isotope diagrams comparing the computed mixing hyperbolae for the best solution (with Dist $< D_{2\sigma}$) and the data. The overall isotopic trend for the high-K lava series is reproduced, to a close approximation, by the calculated hyperbolae. Results for the sedimentary materials are poorly different concerning the isotope ratios (except a lesser radiogenic $^{206}Pb/^{204}Pb$), but greater Sr and Nd and lower Pb concentrations essentially

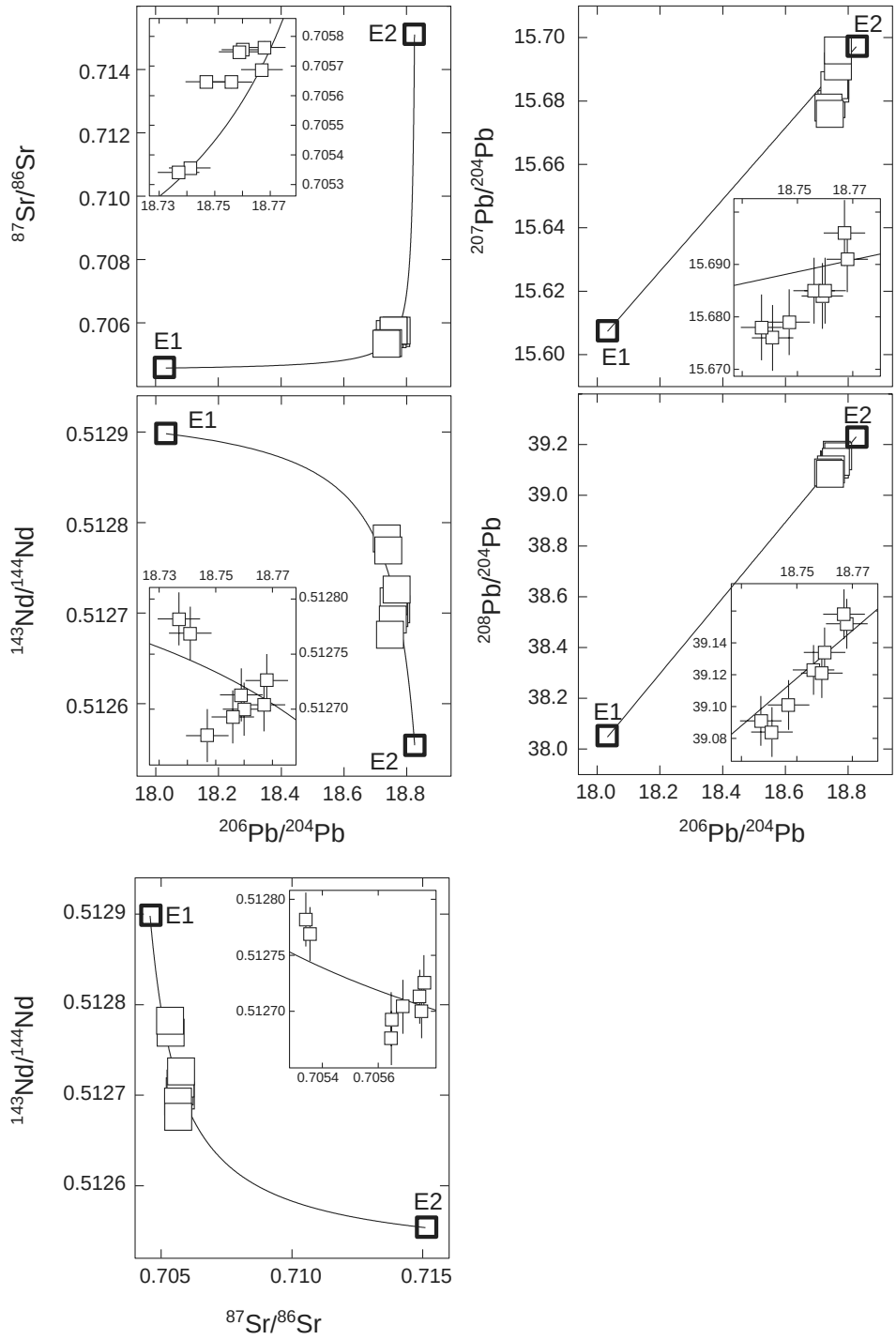

Fig. 10. Isotope diagrams comparing the mixing hyperbola computed for the best solution of a simplified version of the modelling in the five-dimensional isotopic space and data for the high-K lava series from Merapi volcano. Inserts show the error bars (2σ). For this modelling, we have adopted a calculation in which the inputted values of the variables are assumed to be identical to those found for the best solution of the medium-K lava series modelling, except for the sediment-related variables (isotope ratios and trace-element concentrations) which are randomly produced.

explain the dichotomy between the two series. This result gives further support to the hypothesis that compositional differences between the two series encountered at Merapi volcano are mainly inherited from source heterogeneities related to variable contribution of subducted sediments. It also indicates that the system is extremely sensitive to chemical variations in the sedimentary input.

7. Summary

The simplified model of formation of arc lavas described in this study, namely metasomatism of portions of the mantle wedge followed by progressive mixing and melting, is applied successfully to sequences of volcanics from Merapi volcano. The results require a direct relationship

between dehydration of the slab and melting of the metasomatized mantle wedge.

The most important feature of the model is that it generates pseudo-binary mixing trends in isotope diagrams; i.e., the two end-members of these trends do not represent physical components of a subduction zone, but mixtures of derivatives from slab dehydration and melting processes. This feature could reconcile two apparently contradictory observations in some arc settings, namely the evidence from correlations in isotope diagrams that simple binary mixing could generate the range of compositions of arc lavas and the variety of physical processes and potential sources that could be involved in the generation of arc magmas. A corollary to this feature is that caution is required before assessing isotopic compositions of arc lava mantle source components from the isotopic arrays of arc lavas.

Acknowledgments

We thank Claude Maerschalk for his help during preparation and analyses of the samples and Eric Lewin and Ariel Provost for discussion. R.D. and P.S. are also indebted to the Earth Sciences Master 1 students who helped clarify and shape calculations. F. van Wik de Vries helped us for the quality of the manuscript. This paper was improved by critical comments by R. Ellam and R. Gertisser.

Associate editor: Bernard Marty

References

Aizawa, Y., Tastumi, Y., Yamada, H., 1999. Element transport by dehydration of subducted sediments: implication for arc and ocean island magmatism. *The Island Arc* **8**, 38–46.

Allègre, C.J., Hamelin, B., Provost, A., Dupré, B., 1986/1987. Topology in isotopic multispace and origin of mantle chemical heterogeneities. *Earth Planet. Sci. Lett.* **81**, 319–337.

Alves, S., Schiano, P., Allègre, C.J., 1999. Rhenium–Osmium isotopic investigation of Java subduction zone lavas. *Earth Planet. Sci. Lett.* **168**, 65–77.

Alves, S., Schiano, P., Capmas, F., Allègre, C.J., 2002. Osmium isotope binary mixing arrays in arc volcanism. *Earth Planet. Sci. Lett.* **198**, 355–369.

Arculus, R.J., Powell, R., 1986. Source component mixing in the regions of arc magma generation. *J. Geophys. Res.* **91**, 5913–5926.

Ayers, J.C., Eggler, D.H., 1995. Partitioning of elements between silicate melt and H_2O-NaCl fluids at 1.5 and 2.0 GPA pressure; implications for mantle metasomatism. *Geochim. Cosmoschim. Acta* **59**, 4237–4246.

Ben Othman, D., White, W.M., Patchett, J., 1989. The geochemistry of marine sediments, island arc genesis, and crust-mantle recycling. *Earth Planet. Sci. Lett.* **94**, 1–21.

Berthommier P.-C., 1990. Etude volcanologique du Merapi (Centre Java). Téphrostratigraphie et chronologie. Mécanismes éruptifs. Unpublished thesis, University of Clermont-Ferrand.

Bureau, H., Keppler, H., 1999. Complete miscibility between silicate melts and hydrous fluids in the upper mantle: experimental evidence and geochemical implications. *Earth Planet. Sci. Lett.* **165**, 187–196.

Camus, G., Gourgaud, A., Mossand-Berthommier, P.-C., Vincent, P.-M., 2000. Merapi (Central Java, Indonesia): an outline of the structural and magmatological evolution, with a special emphasis to the major pyroclastic events. *J. Volcanol. Geotherm. Res.* **100**, 139–163.

Chadwick, J.P., Troll, V.R., Ginibre, C., Morgan, D., Gertisser, R., Waight, T., Davidson, J.P., 2005. Magma crust interaction at Merapi volcano, Java, Indonesia: insights from crystal isotope stratigraphy. *Geophys. Res. Abstr.* **7**, 06958.

Chauvel, C., Blichert-Toft, J., 2001. A Hafnium isotope and trace element perspective on melting of the depleted mantle. *Earth Planet. Sci. Lett.* **190**, 137–151.

Davidson, J.P., 1987. Crustal contamination versus subduction zone enrichment: examples from the lesser Antilles and implications for mantle source compositions of island arc volcanic rocks. *Geochim. Cosmochim. Acta* **51**, 2185–2198.

Davidson, J.P., Hora, J.M., Garrison, J.M., Dungan, M.A., 2005. Crustal forensics in arc magmas. *J. Volc. Geotherm. Res.* **140**, 157–170.

Davies, J.H., Stevenson, D.J., 1992. Physical model of source region of subduction zone volcanics. *J. Geophys. Res.* **97**, 2037–2070.

Defant, M.J., Drummond, M.S., 1990. Derivation of some modern arc magmas by melting of young subducted lithosphere. *Nature* **347**, 662–665.

DePaolo, D.J., 1981. Trace element and isotopic effect of combined wallrock assimilation and fractional crystallization. *Earth Planet. Sci. Lett.* **53**, 189–202.

Dosso, L., Bougault, H., Beuzart, P., Calvez, J.-Y., Joron, J.-L., 1988. The geochemical structure of the South-East Indian Ridge. *Earth Planet. Sci. Lett.* **88**, 47–59.

Douglass, J., Schilling, J.-G., 2000. Systematics of three-component, pseudo-binary mixing lines in 2D isotope ratio space representations and implications for mantle plume-ridge interaction. *Chem. Geol.* **163**, 1–23.

Edwards, C.M.H., Menzies, M.A., Thirlwall, M.F., 1991. Evidence from Muriah, Indonesia, for the interplay of supra-subduction zone and intraplate processes in the genesis of potassic alkaline magmas. *J. Petrol.* **32**, 555–592.

Edwards, C.M.H., Morris, J.D., Thirlwall, M.F., 1993. Separating mantle from slab signatures in arc lavas using B/Be and radiogenic isotope systematics. *Nature* **362**, 530–533.

Edwards, C.M.H., Menzies, M.A., Thirlwall, M.F., Morris, J.D., Leeman, W.P., Harmon, R.S., 1994. The transition to potassic alkaline volcanism in island arcs: the ringgit-beser complex, East Java, Indonesia. *J. Petrol.* **35**, 1557–1595.

Ellam, R.M., Hawkesworth, C.J., 1988. Elemental and isotopic variations in subduction related basalts: evidence for a three component model. *Contrib. Mineral. Petrol.* **98**, 72–80.

Elliot, T., Plank, T., Zindler, A., White, W., Bourdon, B., 1997. Element transport from slab to volcanic front at the Mariana arc. *J. Geophys. Res.* **102**, 14,991–15,019.

Gerbe, M.-C., Gourgaud, A., Sigmarsson, O., Harmon, R.S., Joron, J.-L., Provost, A., 1992. Mineralogical and geochemical evolution of the 1982–83 Galunggung eruption (Indonesia). *Bull. Volcanol.* **54**, 284–298.

Gertisser, R., Keller, J., 2003a. Trace element and Sr, Nd, Pb and O isotope variations in medium-K and high-K volcanic rocks from Merapi volcano, central Java, Indonesia: Evidence for the involvement of subducted sediments in Sunda arcs magma genesis. *J. Petrol.* **44**, 457–489.

Gertisser, R., Keller, J., 2003b. Temporal variations in magma composition at Merapi Volcano (Central Java, Indonesia): magmatic cycles during the past 2000 years of explosive activity. *J. Volc. Geotherm. Res.* **123**, 1–23.

Gill, J.B., 1981. *Orogenic andesites and plate tectonics*. Springer, New York, 390 pp.

Gill, J.B., Williams, R.W., 1990. Th isotope and U-series studies of subduction related volcanic rocks. *Geochim. Cosmochim. Acta* **54**, 1427–1442.

Hamilton, W., 1979. Tectonics of the Indonesian Region. *U.S. Geol. Survey Prof. Paper* **1078**, 1–345.

Hanan, B.B., Kingsley, R.H., Schilling, J.-G., 1986. Pb isotope evidence in the South Atlantic for migrating ridge-hotspot interactions. *Nature* **322**, 137–144.

Hawkesworth, C.J., Gallagher, K., Hergt, J.M., McDermott, F., 1993. Mantle and slab contributions in arc magmas. *Annu. Rev. Earth Planet. Sci.* **21**, 175–204.

Hemming, S.R., McLennan, S.M., 2001. Pb isotope compositions of modern deep sea turbidites. *Earth Planet Sci. Lett.* **184**, 489–503.

Hofmann, A.W., 1988. Mantle reservoirs. In: Origin of the Earth., Lunar and Planetary Institute, *LPI Contribution* **681**, pp. 33–34.

Hofmann, A.W., 1997. Mantle geochemistry: the message from oceanic volcanism. *Nature* **385**, 219–229.

Hoogewerff, J., Van Bergen, M.J., Vroon, P.Z., Hertogen, J., Wordel, R., Sneyers, A., Nasution, A., Varekamp, J.C., Moens, H.L.E., Mouchel, G., 1997. U series, Sr-Nd-Pb isotope and trace element systematics across an active island arc-continent collision zone: implications for element transfer at the slab-wedge interface. *Geochim. Cosmochim. Acta* **61**, 1057–1072.

Ito, E., Stern, R.J., 1986. Oxygen-isotopic and Strontium-isotopic investigations of subduction zone volcanism ; The case of the volcano arc and the Marianas island-arc. *Earth Planet. Sci. Lett.* **76**, 312–320.

Iwamori, H., 1998. Transportation of H2O and melting in subduction zones. *Earth Planet. Sci. Lett.* **160**, 65–80.

Jonhson, M.C., Plank, T., 1999. Dehydration and melting experiments constrain the fate of subducted sediment. *Geochem. Geophys. Geosyst.* **1**: 1999GC000014.

Kay, R.W., 1978. Aleutian magnesian andesites: Melts from subducted Pacific Ocean crust. *J. Volcanol. Geotherm. Res.* **4**, 117–132.

Kay, R.W., 1980. Volcanic arc magmas: implications of a melting-mixing model for element recycling in the crust-upper mantle system. *J. Geol.* **88**, 497–522.

Keppler, H., 1996. Constraints from partitioning experiments on the composition of subduction-zone fluids. *Nature* **380**, 237–240.

Kersting, A.B., Arculus, R.J., 1995. Pb isotope composition of Klyuchevskoy volcano, Kamchatka and North Pacific sediments: implications for magma genesis and crustal recycling in the Kamchatkan arc. *Earth Planet. Sci. Lett.* **136**, 133–148.

Klein, E.M., Langmuir, C.H., 1987. Global correlations of ocean ridge basalt chemistry with axial depth and crustal thickness. *J. Geophys. Res.* **92**, 8089–8115.

Le Maitre, R.W., Bateman, P., Dudek, A., Keller, J., Lameyer Le Bas, M.J., Sabine, P.A., Schmid, R., Sorensen, H., Streckeisen, A., Woolley, A.R., Zanettin, B., 1989. *A Classification of Igneous Rocks and Glossary of Terms*. Blackwell, Oxford.

McCulloch, M.T., Gamble, J.A., 1991. Geochemical and geodynamical constraint on subduction zone magmatism. *Earth Planet. Sci. Lett.* **102**, 358–374.

McDermott, F., Hawkesworth, C.J., 1991. Th, Pb and Sr isotope variations in young island arc volcanics and oceanic sediments. *Earth Planet. Sci. Lett.* **104**, 1–15.

McLennan, S.M., Taylor, S.R., 1981. Role of subducted sediments in island-arc magmatism: constraints from REE patterns. *Earth Planet. Sci. Lett.* **54**, 423–430.

Miller, D.M., Goldstein, S.L., Langmuir, C.H., 1994. Cerium/lead and lead isotope ratios in arc magmas and the enrichment of lead in the continents. *Nature* **368**, 514–520.

Morris, J.D., Hart, S.R., 1983. Isotopic and incompatible element constraints on the genesis of island arc volcanics from Cold Bay and Amak Island, Aleutians, and implications for mantle structure. *Geochim. Cosmochim. Acta* **47**, 2015–2030.

Nicholls, I.A., Ringwood, A.E., 1973. Effect of water on olivine stability in tholeiites and the production of silica saturated magmas in the island arc environment. *J. Geol.* **81**, 285–300.

Nichols, G.T., Wyllie, P.J., Stern, C.R., 1994. Subduction zone melting of pelagic sediments constrained by melting experiments. *Nature* **371**, 785–788.

Peacock, S.M., 1990. Fluid processes in subduction zones. *Science* **248**, 329–337.

Peacock, S.M., Rushmer, T., Thompson, A.B., 1994. Partial melting of subducting oceanic crust. *Earth Planet. Sci. Lett.* **121**, 227–244.

Perfit, M.R., Gust, D.A., Bence, A.E., Arculus, R.J., Taylor, S.R., 1980. Chemical characteristics of island-arc basalts: implications for mantle sources. *Chem. Geol.* **30**, 227–256.

Pichler, H., Zeil, V.W., 1972. The Cenozoic rhyolite-andesite association of Chilean Andes. *Bull. Volcanol.* **35**, 424–552.

Plank, T., Langmuir, C.H., 1993. Tracing trace elements from sediment input to volcanic output at subduction zones. *Nature* **362**, 739–743.

Plank, T., Langmuir, C.H., 1998. The chemical composition of subducted sediment and its consequences for the crust and mantle. *Chem. Geol.* **145**, 325–394.

Saunders, A.D., Tarney, J., Weaver, S.D., 1980. Transverse geochemical variations across the Antarctic peninsula: implications for the genesis of calc-alkaline magmas. *Earth Planet. Sci. Lett.* **46**, 344–360.

Schiano, P., Allègre, C.J., Dupré, B., Lewin, E., Joron, J.-L., 1993. Variability of trace elements in basaltic suites. *Earth Planet. Sci. Lett.* **119**, 37–51.

Schiano, P., Clocchiatti, R., Shimizu, N., Maury, R.C., Jochum, K.P., Hofmann, A.W., 1995. Hydrous, silica-rich melts in the sub-arc mantle and their relationship with erupted lavas. *Nature* **377**, 595–600.

Schiano, P., Clocchiatti, R., Bourdon, B., Burton, K.W., Thellier, B., 2000. The composition of melt inclusions in minerals at the garnet-spinel transition zone. *Earth Planet. Sci. Lett.* **174**, 375–383.

Schilling, J.-G., Kingsley, R.H., Hanan, B.B., McCully, B.L., 1992. Nd–Sr–Pb isotopic variations along the Gulf of Aden: evidence for Afar mantle plume-continental lithosphere interaction. *J. Geophys. Res.* **97**, 10927–10966.

Stalder, R., Foley, S.F., Brey, G.P., Horn, I., 1998. Mineral-aqueous fluid partitioning of trace elements at 900–1200 °C and 3.0–5.7 GPa: New experimental data for garnet, clinopyroxene, and rutile, and implications for mantle metasomatism. *Geochim. Cosmochim. Acta* **62**, 1781–1801.

Stolper, E., Newman, S., 1994. The role of water in the petrogenesis of Mariana trough magmas. *Earth Planet. Sci. Lett.* **121**, 293–325.

Stolz, A.J., Varne, R., Davies, G.R., Wheller, G.E., Doden, J.D., 1990. Magma source components in an arc-continent collision zone: the Flores-lembata sector, Sunda arc, Indonesia. *Contrib. Mineral. Petrol.* **105**, 585–601.

Tatsumi, Y., Kogiso, T., 1997. Trace element transport during dehydration processes in the subducted oceanic crust: 2.Origin of chemical and physical characteristics in arc magmatism. *Earth Planet. Sci. Lett.* **148**, 207–221.

Tatsumi, Y., Sakuyama, M., Fukuyama, H., Kushiro, I., 1983. Generation of arc basalt magmas and thermal structure of the mantle wedge in subduction zones. *J. Geophys. Res.* **88**, 5815–5825.

Tatsumi, Y., Hamilton, D.L., Nesbitt, R.W., 1986. Chemical characteristics of fluid phase released from a subducted lithosphere and origin of arc magmas: Evidence from high-pressure experiments and natural rocks. *J. Volcanol. Geotherm. Res.* **29**, 293–309.

Tera, F., Brow, L., Morris, J., Selwyn Sacks, I., Klein, J., Middleton, R., 1986. Sediment incorporation in island-arc magmas: Inferences from 10Be. *Geochim. Cosmochim. Acta* **50**, 535–550.

Turner, S.P., Foden, J.D., 2001. U, Th and Ra disequilibria, Sr, Nd and Pb isotope and trace element variations in Sunda arc Lavas: predominance of a subducted sediment component. *Contrib. Mineral. Petrol.* **142**, 43–57.

Turner, S.P., Hawkesworth, C., van Calsteren, P., Heath, E., Macdonald, R., Black, S., 1996. U-series isotopes and destructive plate margin magma genesis in the Lesser Antilles. *Earth Planet. Sci. Lett.* **142**, 191–207.

Turner, S.P., Hawkesworth, C., Rogers, N., Bartlett, J., Worthington, T., Hergt, J., Pearce, J., Smith, I., 1997. $^{238}U/^{230}Th$ disequilibria, magma petrogenesis, and fluxes rates beneath the depleted Tonga-Kermadec island arc. *Geochim. Cosmochim. Acta* **61**, 4855–4884.

Turner, S.P., Foden, J.D., George, R.M., Evans, P., Varne, R., Elburg, M.A., Jenner, G.A., 2003. Rates and processes of potassic magma evolution beneath Sangeang Api volcano, East Sunda Arc, Indonesia. *J. Petrol.* **44**, 491–515.

Varekamp, J.C., Van Bergen, M.J., Vroon, P.Z., Poorter, R.P.E., Wirakusumah, A.D., Erfan, R.D., Suharyono, K., Sriwana, T., 1989. Volcanism and tectonics in the eastern Sunda Arc, Indonesia. *Netherlands J. Sea Res.* **24**, 303–312.

Varne, R., Foden, J.D., 1986. Geochemical and isotopic systematics of Eastern Sunda Arc volcanics: implications for mantle sources and mantle mixing processes the origin of arcs. In: Wezel, F.-C. (Ed.), *The Origin of Arcs*. Elsevier, Amsterdam, pp. 159–189.

Von Drach, V., Marsh, B.D., Wasserburg, G.J., 1986. Nd and Sr isotopes in the Aleutians: multicomponent parenthood of island-arc magmas. *Contrib. Mineral. Petrol.* **92**, 13–34.

Weis D., Frey F.A., 1991. Isotope geochemistry of Ninetyeast Ridge basalt: Sr, Nd and Pb evidence for the involvement of the Kerguelen hot spot, In: Weissel, J., Peirce, J., Taylor, E., Alt, J. (Eds), *Proc. ODP Sci. Research*, **121**, Ocean Drilling Program, College Station, TX, pp. 591–610.

Weis, D., Frey, F.A., 1996. Role of the Kerguelen plume in generating the eastern Indian Ocean seafloor. *J. Geophys. Res.* **101**, 13831–13849.

Weis, D., Kieffer, B., Maerschalk, C., Pretorius, W., Barling, J., 2005. High-precision Pr-Sr-Nd-Hf isotopic characterization of USGS BHVO-1 and BHVO-2 reference materials. *Geochem. Geophys. Geosyst.*. doi:10.1029/2004GC000852.

White, W.M., 1985. Sources of oceanic basalts: radiogenic isotopic evidence. *Geology* **13**, 115–118.

White, W.M., Patchett, P.J., 1984. Hf-Nd-Sr isotopes and incompatible element abundances in island arcs: implications for magma origins and crust-mantle evolution. *Earth Planet. Sci. Lett.* **67**, 167–185.

Woodhead, J.D., 1989. Geochemistry of the Marian arc (Western Pacific): Source composition and processes. *Chem. Geol.* **76**, 1–24.

Woodhead, J.D., Hergt, J.M., Davidson, J.P., Eggins, S.M., 2001. Hafnium isotope evidence for conservative element mobility during subduction zone processes. *Earth Planet. Sci. Lett.* **192**, 331–346.

Wyllie, P.J., 1982. Subduction products according to experimental prediction. *Geol. Soc. Am. Bull.* **93**, 468–476.

Yogodzinski, G.M., Kelemen, P.B., 1998. Slab melting in the Aleutians: implications of an ion probe study of clinopyroxene in primitive adakite and basalt. *Earth Planet. Sci. Lett.* **158**, 53–65.